



Accepted Manuscript











Mineral chemistry, U-Pb zircon ages and tectonic setting of Ariz pluton in the central Iran structural zone (Northern Bafq, Yazd province): Evidence of the Proto-Tethys subduction-related magmatism

Mohsen Hamidi, Mahmoud Sadeghian, Masood Alipour-Asll, Mehdi Rezaei-Kahkhaei, Papadopoulou Lambrini, Maryam Sheibi, Keewook Yi, Hosun Lee, Zhai Mingguo, Foteini Aravani

DOI: 10.22059/geope.2025.396749.648829

Receive Date: 05 June 2025
Revise Date: 04 August 2025
Accept Date: 09 August 2025

Mineral chemistry, U-Pb zircon ages and tectonic setting of Ariz pluton in the central Iran structural zone (Northern Bafq, Yazd province): Evidence of the Proto-Tethys subduction-related magmatism

Mohsen Hamidi ¹, Mahmood Sadeghain ¹, *, Masood Alipour-Asll ¹, Mehdi Rezaei-Kahkhaei ¹, Lambrini Papadopoulou ², Maryam Sheibi ¹, Keewook Yi ³, Hosun Lee ⁴, Zhai Mingguo ⁵, Foteini Aravani ²

¹ Department of Petrology and Economic Geology, Faculty of Earth Sciences, Shahrood University of Technology, Shahrood, Iran

² Department of Mineralogy-Petrology-Economic Geology, School of Geology, Aristotle University, Greece

³ Geochronology Team, Korea Basic Science Institute, Ochang, Republic of Korea

⁴ PNU Core Research Facility, Pusan National University, Busan, South Korea

⁵ Institute of Geology and Geophysics, Chinese Academy of Sciences (CAS), Beijing, China

Received: 05 June 2025, Revised: 04 August 2025, Accepted: 09 August 2025

Abstract

Ariz pluton, covering approximately 65 km², is located 50 to 65 km north of Bafq city, Yazd province, and is part of the central Iran structural zone. This pluton ranges in composition from diorite-quartzdiorite to granodiorite and is characterized by a calc-alkaline, metaluminous nature. These rocks primarily consist of hornblende, biotite, plagioclase, orthoclase and quartz. In this study, for the first time, the chemical compositions of hornblende, biotite, and feldspars are used to determine the physicochemical conditions controlling crystallization, emplacement depth, and tectonic setting. Thermobarometry based on Al-in hornblende and biotite compositions indicates that crystallization and geochemical closure occurred at pressures between 2.8-1.3 kbar and temperatures of 861-713 °C. Most of the amphiboles from the Ariz pluton are indicative of formation in a suprasubduction environment or subduction-related tectonic setting. New obtained zircon U-Pb ages indicate that the rock-forming of Ariz pluton crystallized around Late Neoproterozoic-early Cambrian boundary, representing the final product of the geological events that mainly occurred during the Late Neoproterozoic (Ediacaran). Magma-forming of Ariz pluton probably originated from partial melting of the subducted Proto-Tethys oceanic crust beneath the northern margin of Gondwana supercontinent or its above mantle wedge, during Cadomian orogeny and was emplaced in an active continental margin.

Keywords: Pluton, Thermobarometry, Proto-Tethys, Gondwana, Bafq, Ariz.

Introduction

Thermobarometry is a powerful method for estimating the pressure and temperature conditions of mineral formation in igneous systems and contributes in better understanding of the processes that shape the Earth's crust. Mineral compositions and assemblages in igneous rocks reflect the evolving conditions of the melt during crystallization (Abbott and Clarke, 1979; Helmy et al., 2004). Amphiboles in igneous rocks exhibit significant compositional diversity,

* Corresponding author e-mail: Sadeghian.petrology@gmail.com

which is affected by magma chemistry as well as pressures and temperature conditions during crystallization and cessation of geochemical exchanges (Erdman et al. 2016). However, despite numerous studies on amphibole thermobarometry, including Hammerstrom & Zen (1986), early calibrations of barometers based on the aluminum in hornblende are still useful for near-solidus plutons under specific conditions.

Although the Bafgh-Saghand and Posht-e Badam regions have been extensively studied for the past half century, the area extending from north of Ariz to the northwest of the Chadormalu mine remains understudied due to limited access and challenging terrain. Previous work has focused solely on regional mapping, including the 1:250,000 geological map of Ardekan (Valeh and Haghipour, 1972), and 1:100,000 geological maps of Ariz (Majidi and Babakhani, 2000) and Chadormalu (Ghaemi and Saidi, 2006). This region includes a wide range of igneous and metamorphic rocks dating from the Late Neoproterozoic to Early Cambrian.

Ariz pluton, located at 50 to 65 km north of Bafq, Yazd Province, and in the central Iran structural zone, covering approximately 65 km², ranges in composition from diorite to granodiorite (Figs. 1 and 2a & b). This study is the first to provide comprehensive data on petrography, whole-rock geochemistry, geochronology and mineral chemistry for the Ariz pluton. The aim of this research is to determine the physicochemical conditions governing the crystallization environment and the geochemical closure of this intrusive body in order to determine its age via U-Pb zircon dating method, and identify its formation and tectonic setting.

Geology and petrography

The Late Neoproterozoic-Early Cambrian rocks of Iran have a wide geographical distribution and are present in most of the structural zones of Iran (except Kopeh Dag and Makran). These rocks are mainly exposed in the Central Iran and Sanandaj-Sirjan structural zones and can be divided into two major groups.

The first group comprises igneous and sedimentary rocks that have undergone metamorphism ranging from greenschist to upper amphibolite facies, with ages ranging between about 600 to 530 Ma. The metamorphic rocks include metapelites, metacarbonates, metabasites, and metamorphosed felsic igneous rocks that have been intruded by mainly granitic plutons dated between 560 to 530 Ma. Most of these plutons are S-type biotite-bearing and calc-alkaline in composition. Some of these plutons are as follows: Band e Hezar Chah (Hosseini et al., 2015), Mayamey (Hemmati, 2009; Sadeghian et al., 2017), Sefid-e-Sang (Azizi, 2013); Delbar (Einalou, 2014; Einalou et al., 2014), Chah Jam (Moghadam et al., 2016), North of Aghol-e-Zollou (Rezaei, 2021) in the south and east of Shahrood, Zarrin in the north of Ardakan (Omrani, 1992; Askari, 2021; Askari et al., 2022; Nouri et al., 2021), Bornavard (Sarebani, N., 2017; Karimpour et al., 2011 and Monazzami et al., 2015), Tappeh-e-Taq (north of Eshgh Abad, Tabas) (Rossetti et al., 2015; Mollai et al., 2019), Chah-e-Zard, Kalateh-e-Ghanbar and Airakan in the east of Jandaq to Airakan (Balouchi, 2019; Bagheri and Stampfli, 2008), in the Shahr-e-Kord-Azna belt (Shabani et al., 2018; Davoudian et al., 2022), Moghanlou and Doran in the south of Takab (Esmaeily, 1996; Shafaii Moghadam et al., 2016), Lahijan (south of Lahijan) (Hassanzadeh et al., 2008 and Taki et al., 2013), Khoshoumi (Rashidnejad Omran et al., 2013), Neybaz (Asadi, 2017), Chapedony (Hushmandzadeh, 1969), Kuh Sefid (Ramazan and Tucker, 2003) (southeast of Rabat -e- Posht Badam to the south and west of Saghand).

A smaller subset of these plutons is I-type and calc-alkaline, including parts of the plutons of North Bornavard (Shafaei Moghadam et al., 2017; Karimpour et al., 2011; Sarebani, 2017), Robat Zengijeh (southeast of Tappeh Taq) and the Ariz pluton (study in progress, Figs. 2 to 4). These plutons are considered the youngest units of these complexes. Ariz pluton is the main focus of this study and is considered part of this group. Tectonically, this group represents a

transition from continental rifting to subduction and ultimately the closure of sedimentary basins or continental collision.

Several iron deposits are associated with metamorphic rocks with general metapelitic to metabasitic compositions and in some cases, metacarbonate (Zolala et al., 2025b). Some of these deposits are: Rabat iron deposit (southeast of the Rabat Posht Badam village), Gelmandeh iron deposit (northeast of Saghand), Zaman Abad iron deposit (index under exploration, southeast of the village of Rabat-e-Posht Badam), and Narm and Tengal Sefid iron deposits (Parvaresh Darbandi, 2020). The aforementioned deposits are associated with metapelitic to metabasitic rocks and in some cases metacarbonate. These units are locally overlain by Paleozoic, Mesozoic, Cenozoic sedimentary rocks and Quaternary unconsolidated sediments.

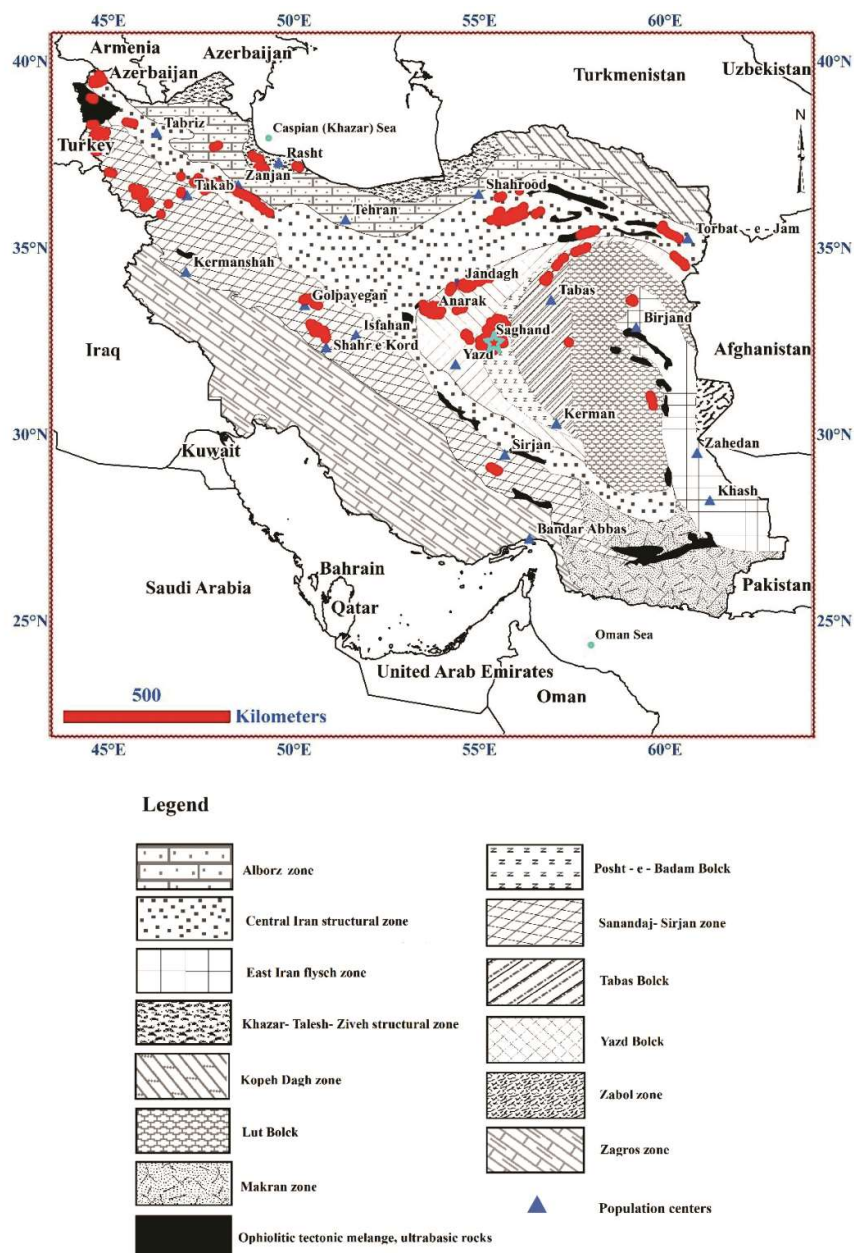
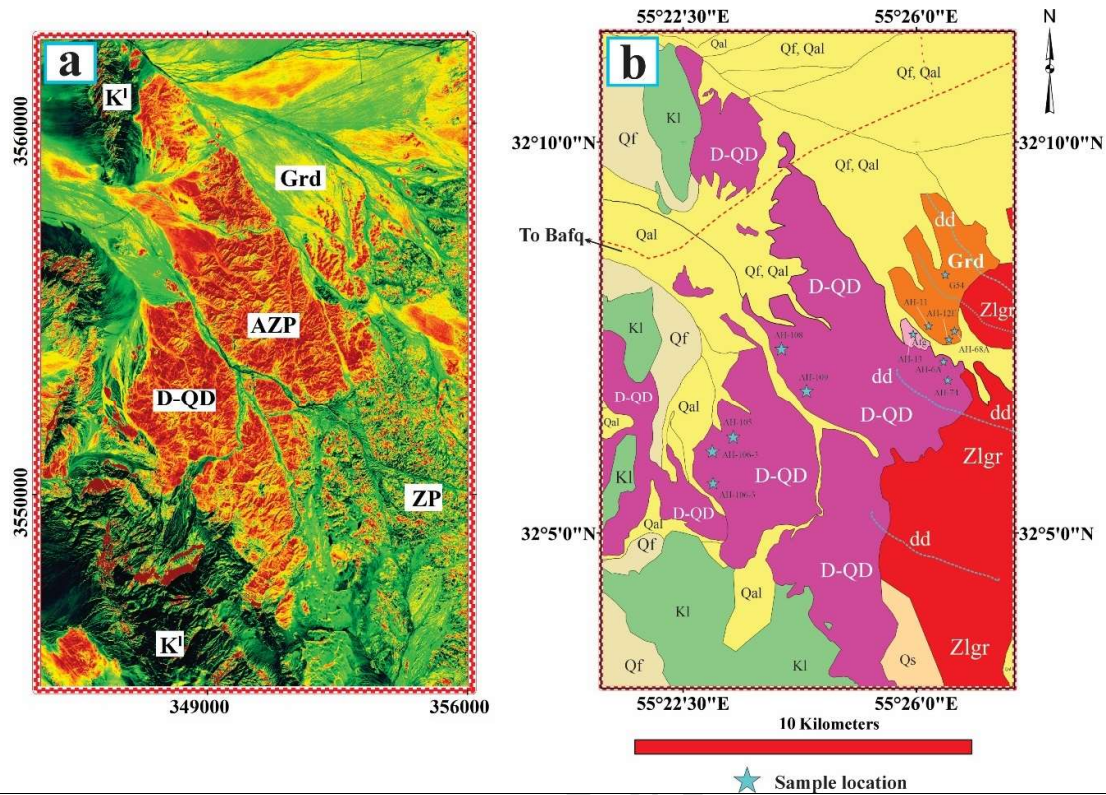


Figure 1. Simplified structural map of Iran (based on Aghanabati, 1998, redrawn by Sadeghian). The study area is located in the central part of Iran, marked with a blue star, between Yazd and Saghand. Red points illustrate Precambrian-early Cambrian outcrops



Selected samples of the Ariz pluton for analysis.

Sample No.	Lithology	X	Y	WHRGCA	MICPA	Zircon U-Pb dating
AH-74	Diorite	55.445°	32.117°		*	
AH-100-1	Diorite	55.378°	32.095°	*		
AH-105	Diorite	55.383°	32.104°			*
AH-106-3	Quartz diorite	55.382°	32.102°	*		
AH-108	Quartz diorite	55.399°	32.117°			*
AH-68	Quartz diorite	55.442°	32.120°	*		
AH-68A	Granodiorite	55.442°	32.120°		*	
AH-109-2	Granodiorite	55.403°	32.113°	*		
AH-11B	Granodiorite	55.434°	32.128°	*	*	*
AH-12E	Granodiorite (+ MME)	55.434°	32.128°	*	*	*
AH-13	Alkali feldspar granite	55.434°	32.126°			

Figure 2. (a) Satellite image of the Ariz pluton (AZP) and its host rocks. Ariz pluton is characterized by an orange-brown colour in the central part of this image. ZP = Zarigan granitic pluton, K¹ = lower Cretaceous fossiliferous limestones and green marls, D-QD= diorite- quartz diorite, Grd = Granodiorite. Pseudocolors were made by the ArcGIS software in symbology windows. (b) Simplified geological map of Ariz pluton. Locations of selected samples are marked with green-blue stars. Zlgr = Zarigan leucogranite, dd = diabasic dikes, Q^s = sand dunes, Q^f = alluvial fans, Q^f & Q^{al} = undifferentiated alluvial fans and stream sediments, K¹ = lower Cretaceous fossiliferous limestones and green marls or in general Cretaceous sedimentary sequence, WHRGCA = Whole rock geochemical analysis, MICPA = Microprobe analysis, Zircon U-Pb Dating, MME = Mafic microgranular enclave. Geographical coordinates are expressed in terms of decimal degrees (DD). For more detailed information, please refer to the main text. Note that to avoid cluttering this figure, diabase dikes (dd) are shown schematically

The second group includes a wide range of igneous rocks (intrusive and extrusive) with bimodal nature (basic and felsic), volcanic-sedimentary and purely sedimentary rocks. These rocks have not been metamorphosed preserving their original texture. In several locations, the traces of Ediacaran and stromatolite fossils are well preserved in sedimentary rocks (Sabzehei et al., 2017). Ediacaran fossils north of the Koushk lead and zinc mine have been studied in detail (Vaziri et al. 2019). The Late Ediacaran age for these deposits is about 539 to 545 Ma for based on the characteristic fossils of *Cloudina* and *Corumbella*. These igneous and sedimentary rocks have been previously classified as the Rizu, Dezu, Raver, Koushk, and Esfordi series, and are interpreted as part of an intracontinental rift (Zolala et al., 2025a). It should be noted that the Late Neoproterozoic-Early Cambrian rocks of the second category in the Zagros structural zone (Hormoz Series) are covered by more than 10 km of thick sedimentary rocks, preventing their exposure on the surface.

Ariz pluton, covering approximately 65 km², is composed mainly of diorite to quartz diorite (about 80%) and granodiorite (about 20%) based on field estimations (Figs. 2 and 3 (a & b)). In addition to green hornblende, granodiorite contains significant amount of biotite. The pluton intruded in predominantly metapelitic rocks (micaschist, garnet mica schist, garnet and andalusite schist), of Late Neoproterozoic age and in less extent metacarbonates (Fig. 3c to f). Field evidence, including the fracturing and the disruption of diorites and quartz diorites by granodiorite bodies, and the presence of mafic microgranular enclaves (MME) and mafic clots (MC) indicates that magma mixing and that the magma forming granodiorites represents a later intrusive phase (Fig. 4b to f). Magma mingling textures can also be observed at a microscopic scale (Fig. 5e & f). In the western part, Zarigan Leucogranite intruded into the Ariz Pluton (Figure 3g). Also, the Ariz pluton was intruded by numerous diabasic dikes (diabasic dike swarm) and also fine-grained pinkish alkali feldspar granites (Fig. 4g and h). Based on the 1:100000 geological map of Ariz (Majidi and Babakhani) and field observations, Ariz pluton, along with its host metamorphic rocks, are overlain unconformably by the Lower and Upper Cretaceous units, including conglomerates, sandstones, green marls, and fossiliferous limestones containing *Orbitulina* and *Orbitoid* (Fig. 3h).

Diorites and quartz diorites

Ariz pluton consists of diorites, quartz diorite and granodiorites (Fig. 3a and b, & Fig. 4), which intruded into the Late Neoproterozoic regional metamorphosed metapelites (micaschist, garnet mica schist, garnet andalusite schist) and metacarbonates (Fig. 3c to f). Numerous diabasic (also known as dolerite) dikes that cut the Zarigan pluton also continue within the diorites and quartz diorites, cross-cutting them (Fig. 3b & g). Due to their similar color, distinguishing diabasic dikes from the surrounding diorites and quartz diorites is difficult in the field and requires careful field observation (see Fig. 3b, and Fig. 4g). Where these dikes cut through the Zarigan leucogranite, they are easily identified and traced in outcrops and satellite images due to their large color contrast (Fig. 3g). These dikes are numerous, reaching hundreds, perhaps even more than one thousand, and are best described as diabasic dike swarms (Tajbakhsh, 2020; Tajbakhsh et al., 2023). It should be noted that to avoid cluttering the figure, diabase dikes (dd) are shown schematically in Figure 2b. Meanwhile, a few pinkish alkali feldspar granitic dikes and small intrusions intruded into diorites and quartz diorites (Figs. 2b and 4h).

These rocks have a medium-grained granular to porphyroïdic texture, and their primary minerals are plagioclase and green hornblende (Fig. 5). Plagioclase forms euhedral to subhedral grains exhibiting polysynthetic twinning and mixed zoning, and in some cases, altered to sericite and clay minerals. Green hornblende is abundant in these rocks, forming euhedral and subhedral unaltered crystals. Biotite, orthoclase, and quartz are found in smaller amounts in these rocks. In some cases, green hornblende is associated with biotite. Quartz is anhedral and fills the spaces

between other minerals. Sphene (titanite), magnetite, titanomagnetite, zircon and apatite are the accessory minerals of these rocks. Opaque minerals are present in minor amounts and are usually found as subhedral to anhedral grains (Fig. 5a to f). The porphyroidic texture observed in these rocks indicates crystallization at relatively shallow depths or upper crustal levels (Fig. 5c). Magma mingling and mixing evidence was observed in the form of microgranular mafic enclaves and mafic clots at a macroscopic scale or field observations (Fig. e & f).

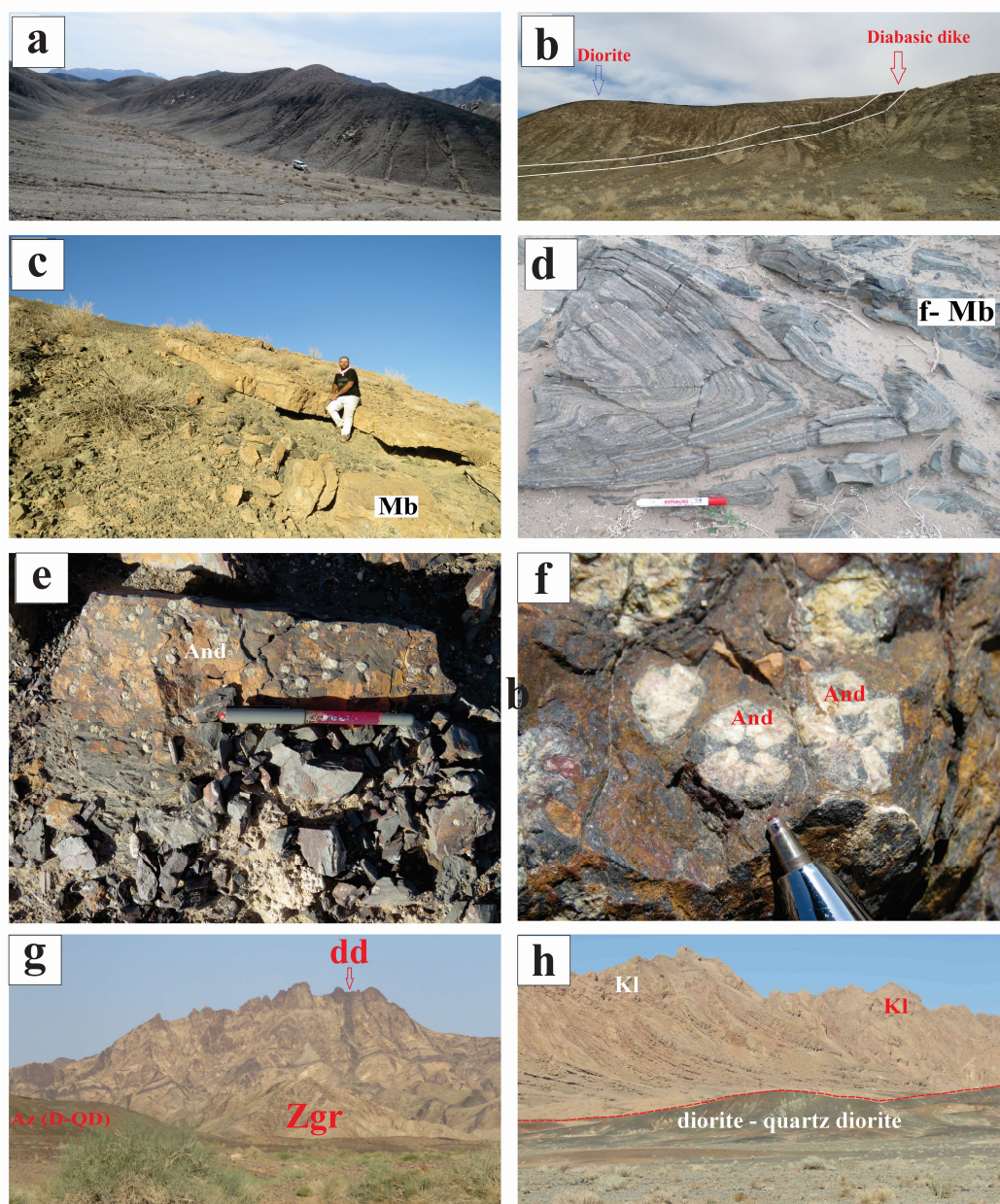


Figure 3. a - Diorites and quartz diorites (Az (D-QD)) with gentle and hilly morphology are visible in the front part of the image. b - Diabasic dike cutting the dioritic rocks of the Ariz pluton. c - Metacarbonates (calcitic marbles) as a host rock of the Ariz pluton. d - close view of folded metacarbonates or marble (f-Mb). e - Garnet and andalusite schist (metapelite) as a host rock of this pluton. f - close view of garnet and andalusite schist. Andalusite (And) is characterized by chiasolite structure. g - Diabasic dike swarms (dd) cutting Zarigan pluton (Zgr), diorite and quartz diorite of Ariz pluton are visible in the front of the picture (in the left corner). h - The contact of diorite and quartz diorites with lower Cretaceous fossiliferous limestones (K^l) at the western border of Ariz pluton. This boundary is of the nonconformity type

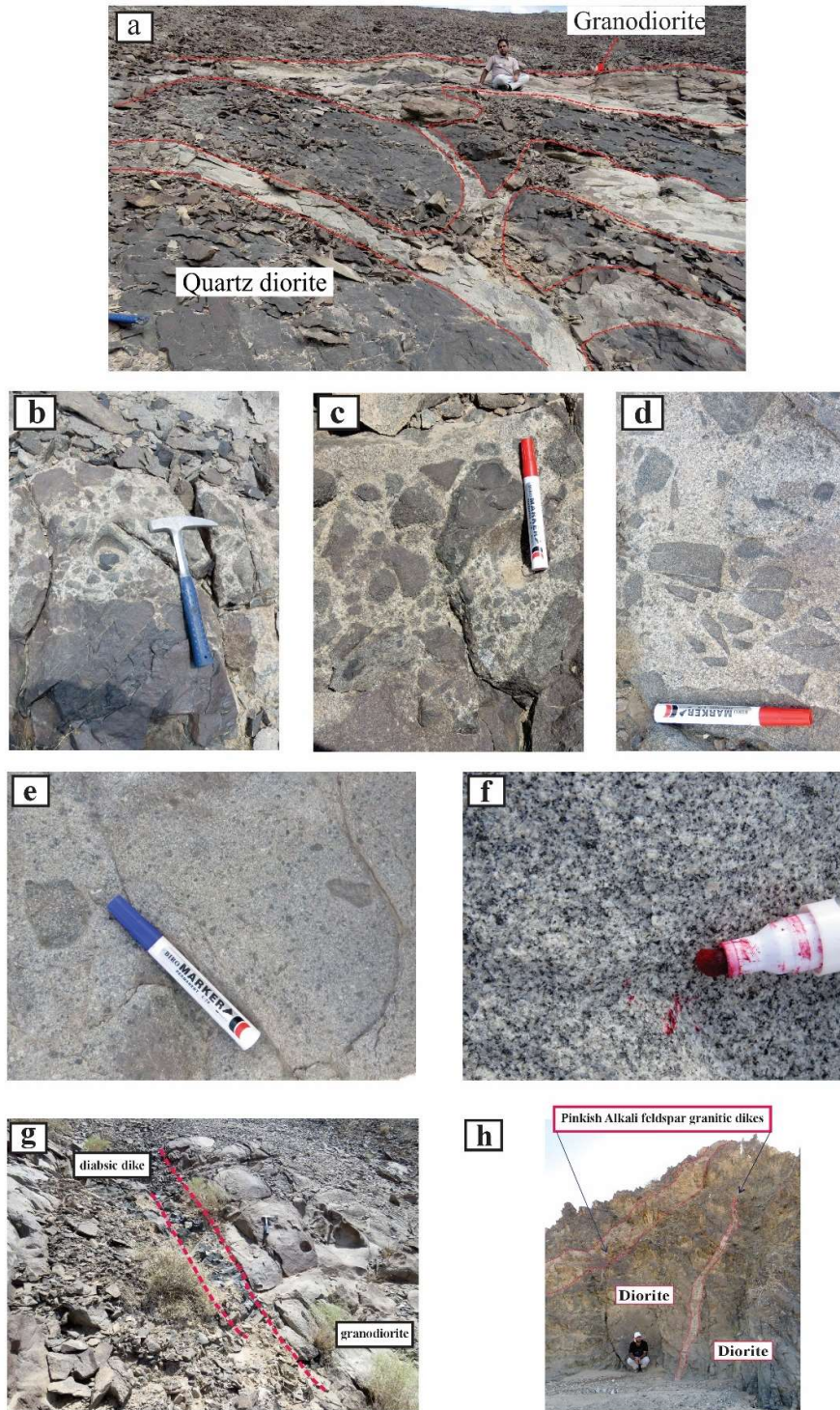


Figure 4. Field photos of relationships between quartz diorite, granodiorite and cutting diabasic dikes at location with X= 352286 or 55.434°, and Y= 3555688 or 32.128° coordination (in terms of UTM (Zone 40 N) and decimal degrees). (a) fragmentation of diorite and quartz diorites by granodiorite (more felsic magma and with light colour); a dark, mafic magma interacting with a light, felsic magma. Some of the interactions clearly suggest the mafic magma was cool enough to form angular blocks. (b to f) magma mingling and magma mixing evidence of diorite-quartz diorite and granodiorite, (e) mafic microgranular enclaves and mafic clots in granodiorites, (f) close view of granodiorites; (g) diabasic dikes cut granodiorites; (h) fine-grained pinkish alkali feldspars dikes were intruded in dioritic rocks of the Ariz pluton

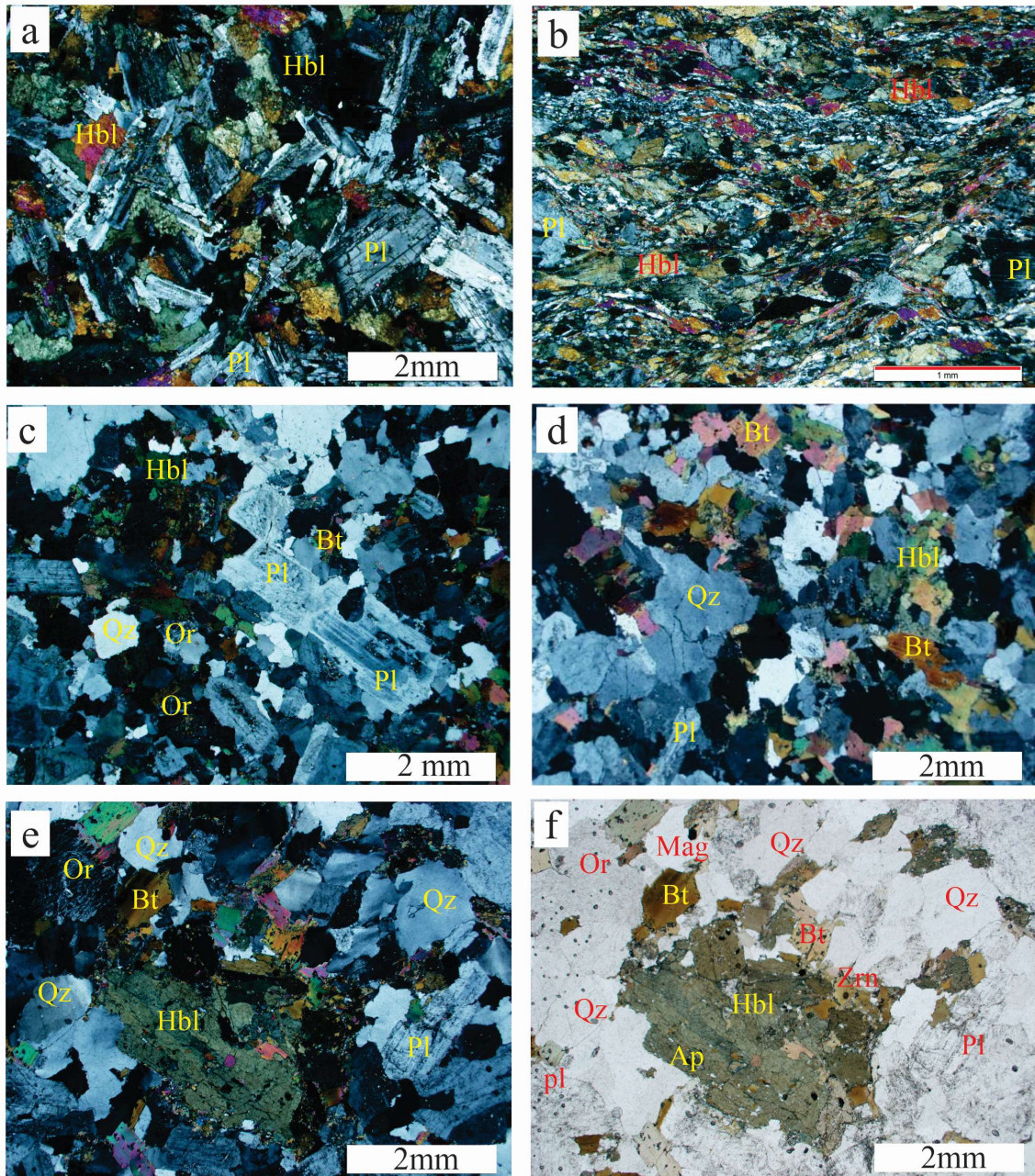


Figure 5. Photomicrographs of the Ariz quartz diorites and granodiorites. (a) Diorites, (b) Development of mylonitic microstructures in locally mylonitised quartz diorites, such as foliation and subgraining. (c & d) Granodiorite with granular texture. (e & f) Mafic clots include hornblende, biotite, apatite, and zircon. Hbl= Hornblende, Bt = Biotite, Pl = Plagioclase, Or = Orthoclase, Qz = Quartz, Ap = Apatite, Mag = Magnetite, Zrn = Zircon. Abbreviations are after Warr (2021)

Diorites and quartz diorites have undergone mylonitization along several shear zones (Fig. 5b). These zones are characterized in the field by foliation and development of S- and C-type shear surfaces and can be observed on scales ranging from a few square centimeters to a few tens of square meters. However, due to the dark green to black color of the rocks, identifying these mylonitic or shear zones requires more and more attention. Characteristic microstructures of mylonites (Passchier et al., 2005; Trouw et al., 2009) are present in these rocks and include subgraining, bulging, grain boundary migration, oblique orientation and mantle porphyroclasts such as σ - and δ -clasts and fish-shaped hornblende, plagioclase and mica clasts (see Fig. 5b).

In some cases, mylonitization and circulation of aqueous fluids is resulted in alteration of the minerals with development of actinolite, chlorite, epidote, calcite and sericite within the shear zones. Metamorphic conditions in these zones locally reached greenschist to lower amphibolite facies. Magma mixing evidence was observed in the form of mafic clots at a microscopic scale (Fig. 5e & f). Nearby metacarbonates, exposed at the contact between the intrusive diorites/quartz diorites and country rocks, have undergone relatively advanced contact metamorphism as evidenced by recrystallization. It should be noted that these metamorphic rocks are very sparsely distributed and also have small outcrops; therefore, they are not mappable in large-scale geological maps. For this reason, those are not shown in the geological map (Fig. 2).

Granodiorites

Granodiorites are distinguished in the field by their lighter color and more distinct grain structure than diorites and quartz diorites. The modal abundance of felsic minerals (plagioclase, orthoclase, and quartz) is higher than that of mafic minerals (green hornblende and biotite). However, biotite in these rocks is significantly more abundant than in diorites and quartz diorites. Sphene, magnetite, titanomagnetite, zircon, and apatite are found as accessory minerals in these rocks which have granular texture (Fig. 5c & d). An interesting feature of these rocks is the presence of microgranular mafic enclaves, mafic clots composed of hornblende and biotite (on a millimeter scale), which are indicative of magma mixing between the magmas forming diorites – quartz diorites and granodiorites. Biotite occurs as isolated crystals, sometimes in contact with euhedral to subhedral hornblende and it contains inclusions of the opaque minerals (magnetite and titanomagnetite) and apatite. Plagioclases are abundant in these rocks and appear as subhedral to anhedral crystals with zoning and polysynthetic twinning. Potassium feldspars usually show Carlsbad twinning and perthitic texture. Quartz is relatively abundant and is often observed as subhedral to anhedral grains. Magnetite, titanomagnetite, apatite, and zircon are found as inclusions in the aforementioned minerals (see Fig. 5e & f). As mentioned earlier, magma mixing evidence was observed in the form of mafic clots at a microscopic scale (Fig. 5e & f).

Analytical methods

A - Whole-rock geochemistry

Six samples of the Ariz pluton (diorite-quartz diorite and granodiorite) were collected and analyzed for major and trace elements using inductively coupled plasma (ICP) spectroscopy. 20.0 g of rock powder were melted with 1.5 g of LiBO₂ and dissolved in 100 ml of 5% nitric acid. Thermal loss was determined by drying the samples at 1000°C. Rare earth element (REE) analysis was performed using ICP-MS at ACME Laboratory in Vancouver, Canada. The detection limits are 0.1 to 0.01 wt.% for major oxides, 10 to 0.1 ppm for trace elements, and 0.5 to 0.01 ppm for rare trace elements. The chemical analysis of rock samples from the Ariz pluton is given in Table 1.

B- Microprobe analyses

Approximately 120 hand specimens were collected from the Ariz pluton and its host rocks. Four samples of the least altered rocks were prepared for thin-section and microprobe analysis, including two diorite-quartz diorite samples (AH-68A and AH-74) and two granodiorite samples (AH-11 and AH-12E). Microprobe analysis was performed using a scanning electron

microscope (SEM), JEOL JSM-840A model, equipped with an energy dispersive spectrometer (EDS, Oxford INCA 250) at the Aristotle University of Thessaloniki, Greece. Instrument settings during analysis included an accelerating voltage of 20 kV with a beam current of 0.4 mA and a time interval of 40 seconds. A pure Co standard was used for instrument calibration. For SEM studies, samples were coated with carbon to a thickness of 200 Angstroms (Å). The JEOL JSM-840A vacuum evaporator has a detection limit of 0.6 to 0.2 wt.%. The cation numbers of amphibole, biotite, and plagioclase were calculated using Minpet 2.02 software and other spreadsheet software available in Excel, based on 23, 11, and 8 oxygens, respectively (Supplementary Tables 2, 3, and 4).

Table 1. Selected samples of the Ariz pluton for whole rock geochemical analysis

Sample No.	AH-100-1	AH-106-3	AH-11B	AH-109-2	AH-68	AH-12E
Lithology	D	Q-D		Grd		
X	55.378°	55.382°	55.434°	55.403°	55.442°	55.434°
Y	32.095°	32.102°	32.128°	32.113°	32.120°	32.128°
SiO ₂ (wt.%)	53.52	55.98	68.06	68.9	70.29	72.65
TiO ₂	0.65	0.68	0.38	0.51	0.3	0.55
Al ₂ O ₃	17.09	16.08	14.17	14.69	13.85	13.36
Fe ₂ O ₃	8.87	8.23	4.56	4.13	3.83	2.93
Cr ₂ O ₃	0.019	0.019	0.026	0.022	0.021	0.025
MgO	4.88	4.73	1.44	0.98	1.15	0.77
MnO	0.17	0.16	0.06	0.06	0.03	0.06
CaO	9.06	8.28	3.46	4.24	2.71	2.03
Na ₂ O	2.67	2.31	3.33	3.23	3.41	3.6
K ₂ O	1.02	1.35	3.34	2.83	3.52	3.13
P ₂ O ₅	0.14	0.13	0.07	0.09	0.05	0.08
TOT/C	0.18	0.09	0.02	0.06	0.03	0.07
TOT/S	<0.02	<0.02	<0.02	<0.02	<0.02	<0.02
LOI	1.7	1.8	0.8	1.4	0.8	1.4
Sum	99.8	99.81	99.91	99.89	99.92	99.88
Rare earth elements (ppm)						
La	10.8	12.5	25.1	27.1	30.1	8.5
Ce	21.4	28	52.5	54.7	60.8	17.6
Pr	2.61	3.15	5.69	6.14	6.22	2.13
Nd	10.4	12.2	22.4	24.1	21.2	9.5
Sm	2.39	2.75	4.08	4.91	4.14	2.57
Eu	0.73	0.67	0.77	0.83	0.6	1.04
Gd	2.57	3.07	4.49	5.12	3.85	3.02
Tb	0.38	0.46	0.74	0.83	0.59	0.53
Dy	2.38	2.75	4.64	4.86	3.63	3.14
Ho	0.46	0.61	1.03	1.07	0.79	0.65
Er	1.5	1.87	3.06	3.07	2.44	1.97
Tm	0.23	0.24	0.45	0.45	0.35	0.25
Yb	1.43	1.72	2.92	3.03	2.33	1.64
Lu	0.21	0.27	0.49	0.47	0.38	0.24
Y	12.3	16	27.4	28.4	20.9	17.4

D-QD = Diorite – Quartz diorite

Grd = Granodiorite

Geographical coordinates are expressed in terms of decimal degrees (DD).

Table 1. Continued

Sample No.	AH-100-1	AH-106-3	AH-11B	AH-109-2	AH-68	AH-12E
Lithology	D	Q-D	Grd			
X	55.378°	55.382°	55.434°	55.403°	55.442°	55.434°
Y	32.095°	32.102°	32.128°	32.113°	32.120°	32.128°
Ba	364	472	577	736	469	510
Be	1	1	1	2	<1	<1
Co	25.1	22.6	6	8	4.4	6.7
Cs	1.3	0.8	1.9	1.4	1.7	1
Ga	14.9	14.4	14	14.7	13.6	16
Hf	1.1	3	5.5	6	5.3	8.8
Nb	3.3	4.8	6.3	6.5	6.9	4.1
Rb	23.1	38.1	92.2	81.3	92.2	37.3
Sc	30	29	10	12	7	12
Sn	<1	<1	1	<1	1	<1
Sr	360.2	292.7	124.7	168	97.1	243.6
Ta	0.2	0.3	0.6	0.6	0.7	0.3
Th	0.7	2.1	14.1	10.1	20.4	0.6
Ti	3900	4080	2280	3060	1800	3300
U	0.2	0.2	2.8	1.3	2.6	0.4
V	273	243	58	74	36	51
W	1.1	0.6	0.6	<0.5	<0.5	<0.5
Zr	41	99.7	182.9	213.3	166	350
Ag	<0.1	<0.1	<0.1	<0.1	<0.1	<0.1
Au (ppb)	2.5	2.9	0.7	<0.5	0.6	0.6
As	<0.5	0.7	1	0.6	0.9	<0.5
Bi	<0.1	<0.1	<0.1	<0.1	<0.1	<0.1
Cu	41.9	39.5	14.2	5.9	8.8	14.4
Cd	<0.1	<0.1	<0.1	<0.1	<0.1	<0.1
Hg	<0.01	<0.01	<0.01	<0.01	<0.01	<0.01
Mo	0.3	1.2	0.4	2	0.4	2
Ni	14.1	21.3	7.2	7.7	5.6	5.8
Pb	7.3	10.6	4.9	4.1	6	8.9
Sb	<0.1	<0.1	<0.1	<0.1	<0.1	<0.1
Se	<0.5	<0.5	<0.5	<0.5	<0.5	<0.5
Tl	0.1	0.2	0.3	0.3	0.3	0.2
Zn	67	87	34	30	21	50

D-QD = Diorite – Quartz diorite

Grd = Granodiorite

C- U-Pb isotopic analysis

U-Pb isotopic analysis was performed using the SHRIMP instrument at the Korea Institute of Basic Sciences, South Korea. At first, zircon grains separated from these rocks were mounted in epoxy resin and then polished up to reveal their internal structures. Before measuring the U-Th-Pb isotopic compositions, microscopic images were taken in transmitted light, reflected light and also cathodoluminescence or backscatter images to identify suitable points for analysis. The isotopic analysis methods were based on the methods of Williams (1998) and McKibben et al. 1988 (Table 5). The data obtained were processed and evaluated using SQUID 1.02 (Ludwig, 2001) and Isoplot 3.0 (Ludwig, 2003) software. Common lead is corrected based on the measured ^{207}Pb value. Uncertainties in the measured compositions of the primary

standard have been calculated to obtain uncertainties in the $^{207}\text{Pb}/^{236}\text{U}$ ages of diorites and quartz diorites, as well as granodiorites of the Ariz pluton, by calculating the square root of some of the individual square deviations.

Results

Nomenclature and determination of magma series

A TAS diagram, or Total Alkali Silica diagram (such as Cox et al., 1979; Middlemost, 1985; & Middlemost, 1994), is a classification tool used in igneous petrology to categorize intrusive igneous rocks based on their chemical composition, specifically the weight percentages of silica (SiO_2) and total alkalis ($\text{Na}_2\text{O} + \text{K}_2\text{O}$). It's a simple X-Y plot where the composition of an igneous rock sample is plotted, and the region it falls into indicates its rock type. Rocks forming of Ariz pluton in these diagrams (Fig. 6a, b & c) fall into gabbrodiorite, diorite, quartz diorite, granodiorite and granite fields.

Table 2. Selected EPMA analytical data of amphiboles were calculated based on 23 oxygen atoms in the structural formula

the structural formula													
Sample NO.	AH-68A				AH-74			AH-11			AH-12-E		
	D-QD							Grd					
SiO2	50.8	50.1	48.1	49.4	48.3	50.7	50.6	47.3	49.0	47.8	45.8	50.1	
TiO2	0.5	1.0	1.0	1.9	1.6	1.4	1.1	1.4	1.1	0.6	0.5	1.1	
Al2O3	5.5	7.1	7.7	6.9	7.3	6.5	6.0	8.5	6.4	7.3	7.5	6.4	
FeO	18.4	19.2	18.9	14.4	15.0	15.3	17.2	17.4	17.8	19.2	20.6	18.4	
MnO	0.8	0.3	0.8	0.2	0.5	0.3	0.3	0.5	0.4	0.7	0.7	0.1	
MgO	9.3	7.9	8.3	12.0	11.9	11.6	9.9	9.9	10.6	10.0	9.6	9.8	
CaO	10.5	10.1	10.2	10.1	10.5	10.3	9.8	10.1	10.6	9.7	9.5	10.1	
Na2O	1.1	1.2	1.3	1.4	1.6	1.2	0.5	1.0	0.9	0.9	2.2	1.1	
K2O	0.9	0.6	0.8	1.0	0.7	0.8	2.4	1.0	0.8	0.8	0.6	0.7	
Total	97.7	97.6	97.6	97.3	97.5	98.2	98.1	97.7	97.7	97.1	97.5	98.2	
Si	7.5	7.4	7.2	7.2	7.1	7.4	7.5	7.1	7.3	7.2	7.0	7.4	
Al	1.0	1.2	1.4	1.2	1.3	1.1	1.0	1.5	1.1	1.3	1.4	1.1	
Fe3+	0.0	0.0	0.0	0.0	0.0	0.0	0.0	0.0	0.0	0.0	0.0	0.0	
Fe2+	2.3	2.5	2.4	1.8	1.9	1.9	2.2	2.2	2.2	2.4	2.7	2.3	
Ti	0.1	0.1	0.1	0.2	0.2	0.2	0.1	0.2	0.1	0.1	0.1	0.1	
Cr	0.0	0.0	0.0	0.0	0.0	0.0	0.0	0.0	0.0	0.0	0.0	0.0	
Mg	2.1	1.8	1.9	2.6	2.6	2.5	2.2	2.2	2.3	2.3	2.2	2.2	
Mn	0.1	0.0	0.1	0.0	0.1	0.0	0.0	0.1	0.0	0.1	0.1	0.0	
Ca	1.7	1.6	1.6	1.6	1.7	1.6	1.6	1.6	1.7	1.6	1.6	1.6	
K	0.2	0.1	0.1	0.2	0.1	0.2	0.4	0.2	0.1	0.1	0.1	0.1	
Na	0.3	0.4	0.4	0.4	0.5	0.3	0.1	0.3	0.2	0.3	0.7	0.3	
Total	15.2	15.1	15.3	15.3	15.4	15.2	15.2	15.3	15.3	15.3	15.7	15.2	
P †		2.5	2.8	2.3	2.6	2.1	2.0	3.2	2.1	2.6	2.7	2.1	
T ♦		792.6	792.6	850.4	839.6	834.6	825.3	831.7	818.0	755.9	744.2	785.0	

† Al-in-Hbl barometer (kbar) by Mutch et al. (2016)

♦ Amp-liq thermometer (°C) by Putirka (2016; Eqn. 4b)

D-QD = Diorite – Quartz diorite

Grd = Granodiorite

Table 3. Selected EPMA analytical data of biotites (Mica) were calculated based on 11 oxygen atoms in the structural formula

in the structural formula												
Sample No.		AH-68A-& 74					AH-11			AH-12E		
Lithology		D-QD					Grd					
SiO2	36.47	37.44	36.63	37.64	37.34	37.01	36.73	37.84	37.16	37.15	38.37	37.61
TiO2	3.01	2.88	3.56	1.83	3.85	1.55	2.76	2.86	3.40	3.73	2.53	1.93
TiO2-10	30.09	28.83	35.56	18.34	38.53	15.54	27.65	28.65	34.05	37.33	25.35	19.28
Al2O3	15.86	14.78	15.56	14.92	15.52	17.33	16.22	14.10	15.16	15.36	16.18	14.84
FeO	22.21	18.35	19.56	18.72	17.67	20.88	19.73	19.58	20.44	20.54	20.87	23.10
MnO	0.49	-	-	0.25	-	-	0.09	0.58	0.37	0.33	-	0.30
MgO	7.92	12.20	10.54	11.97	11.52	9.12	9.82	9.96	8.74	8.22	7.90	7.52
CaO	0.21	-	0.03	-	0.33	0.21	0.09	0.12	0.22	0.31	-	-
Na2O	0.61	-	-	0.60	0.16	0.46	-	0.25	-	-	-	-
K2O	8.96	9.57	9.50	9.28	9.05	9.00	9.76	9.70	9.68	9.48	9.54	9.84
Cl	0.27	0.78	0.64	0.67	0.57	0.44	0.66	0.83	0.67	0.50	0.31	0.44
Sum	96.00	96.00	96.01	95.89	96.01	96.00	95.86	95.82	95.85	95.62	95.71	95.57
O=Cl	0.06	0.18	0.14	0.15	0.13	0.10	0.15	0.19	0.15	0.11	0.07	0.10
Total	95.94	95.82	95.86	95.74	95.88	95.91	95.71	95.63	95.70	95.51	95.64	95.47
Si	5.61	5.66	5.56	5.70	5.60	5.62	5.60	5.79	5.69	5.69	5.83	5.84
Ti	0.35	0.33	0.41	0.21	0.43	0.18	0.32	0.33	0.39	0.43	0.29	0.22
Al ^{VI}	0.48	0.29	0.35	0.37	0.35	0.72	0.51	0.33	0.43	0.47	0.73	0.55
Al ^{IV}	2.39	2.34	2.44	2.30	2.40	2.38	2.40	2.21	2.31	2.31	2.17	2.16
Alttotal	2.87	2.63	2.79	2.66	2.74	3.10	2.91	2.54	2.74	2.77	2.90	2.71
Fe2	2.86	2.32	2.48	2.37	2.22	2.65	2.51	2.50	2.62	2.63	2.65	3.00
Mn	0.06	0.00	0.00	0.03	0.00	0.00	0.01	0.08	0.05	0.04	0.00	0.04
Mg	1.82	2.75	2.39	2.70	2.58	2.07	2.23	2.27	2.00	1.88	1.79	1.74
Ca	0.04	0.00	0.00	0.00	0.05	0.03	0.01	0.02	0.04	0.05	0.00	0.00
Na	0.18	0.00	0.00	0.18	0.05	0.14	0.00	0.07	0.00	0.00	0.00	0.00
K	1.76	1.84	1.84	1.79	1.73	1.74	1.90	1.89	1.89	1.85	1.85	1.95
Cl	0.07	0.20	0.17	0.17	0.15	0.11	0.17	0.22	0.17	0.13	0.08	0.12
Nr of O	22.00	22.00	22.00	22.00	22.00	22.00	22.00	22.00	22.00	22.00	22.00	22.00
Ratio O/Sum	9.24	9.08	9.13	9.10	9.02	9.13	9.16	9.19	9.20	9.21	9.13	9.32
D-QD = Diorite – quartz diorite						Grd = granodiorite						

D-QD = Diorite – quartz diorite

Grd = granodiorite

The R1-R2 chemical variation diagram (De La Roche et al., 1980), which includes all of the major cations, a mineralogical network, the degree of silica saturation, and the combined changes in Fe/(Fe+Mg) and (Ab+Or)/An ratios in igneous rocks, is proposed where: X or R1 = $4\text{Si} - 11(\text{Na}+\text{K}) - 2(\text{Fe}+\text{Ti})$ and Y or R2 = $6\text{Ca} + 2\text{Mg} + \text{Al}$. R1 and R2 are parameters calculated either from chemical analyses (oxide percentages converted to milliequivalents) or modal data. Based on this diagram (Fig. 6d), samples of the Ariz pluton fall into quartz diorite and granodiorite fields.

But with respect to petrographic consideration, such as ubiquity of hornblende, quartz modal frequency, and lack of pyroxene, it's better to limit their classification in diorite-quartz diorite and granodiorite terms or domains. Also, Ariz pluton rocks have subalkaline, calc-alkaline, high-potassium calc-alkaline, and metaluminous nature ($\text{K}_2\text{O}-\text{SiO}_2$ and $\text{Al}_2\text{O}_3/(\text{Na}_2\text{O}+\text{K}_2\text{O})-\text{Al}_2\text{O}_3/(\text{CaO}+\text{Na}_2\text{O}+\text{K}_2\text{O})$ diagrams (Fig. 6e & f).

Harker diagrams (1909) are graphical tools used in geochemistry, specifically in igneous petrology, to analyze variations in major and trace element concentrations within a suite of rocks, typically plotted against silica (SiO_2) as a differentiation index. These diagrams help

understand magmatic processes like fractional crystallization and magma mixing. Harker variation diagrams for Ariz pluton reveal a general decrease in Al_2O_3 , MgO , CaO , FeO , TiO_2 and P_2O_5 contents with increasing SiO_2 , and also an increase in Na_2O and K_2O . The distribution behavior of trace elements during magmatic differentiation can be traced by their variations with increasing SiO_2 . Harker diagrams for trace elements also reveal a general increase in Ba, Cs, Zr, La, Ce, Y and Rb (from LILE and HSFE groups, and incompatible elements) contents with increasing SiO_2 . On the other hand, indicate a usual decrease in Sr, Sc, Ni, Co and V (compatible elements) contents with increasing SiO_2 . In the first sight, it looks like there is a geochemical gap between diorite-quartz diorite and granodiorites. But, indeed, this gap is solely caused by the low number of selected samples for geochemical analysis. Because the studied rocks have very close relationships in the field and their mineral assemblages are very close to each other. In fact, all of these variation diagrams with linear trend confirmed fractional crystallization that took place during magma evolution procedures (decreasing mafic minerals and increasing felsic minerals) and indicate that the studied rocks are cogenetic. This gap should not be considered as a compositional bimodality.

Table 4. Selected EPMA analytical data of feldspars (orthoclase and plagioclase) were calculated based on 8 oxygen atoms in the structural formula

Sample NO.	Lithology	Mineral type	Ab (Na)	Or (K+Ba)	An (Ca+Mn+Mg)
AH-74-C1	D-QD	Flds (Plg)	75.7	0.6	23.7
AH-74-C1	D-QD	*	74.9	0.0	25.1
AH-74-C1	D-QD	*	63.0	0.5	36.5
AH-74-C1	D-QD	*	54.6	0.3	45.0
AH-68A-C4	D-QD	*	77.8	0.0	22.2
AH-68A-C4	D-QD	*	66.1	0.5	33.4
AH-68A-C4	D-QD	*	65.3	0.8	34.0
AH-68A-C4	D-QD	*	78.3	0.6	21.1
AH-68A-C4	D-QD	*	69.7	0.2	30.1
AH-68A-C4	D-QD	*	76.6	1.5	21.9
AH-68A-C4	D-QD	*	68.5	1.2	30.3
AH-68A-C4	D-QD	*	54.8	0.2	45.0
AH-68A-C1	D-QD	*	6.5	93.3	0.2
AH-68A-C1	D-QD	*	8.5	89.4	2.1
AH-68A-C1	D-QD	*	8.6	91.1	0.3
AH-68A-C1	D-QD	*	7.4	92.1	0.4
AH-68A-C4	D-QD	*	2.8	96.7	0.6
AH-11-C5	Grd	*	3.6	95.6	0.8
AH-11-C6	Grd	*	6.0	94.0	0.0
AH-12-C2	Grd	*	6.3	93.7	0.0
AH-12-C2	Grd	*	26.5	73.4	0.1
AH-12-C3	Grd	*	4.5	95.0	0.5
AH-12-C3	Grd	*	5.8	93.6	0.6
AH-12-C3	Grd	*	12.7	87.0	0.3
AH-12-C1	Grd	*	6.4	93.5	0.2
AH-12-C1	Grd	*	30.2	69.8	0.0
AH-68A-C1	Grd	Flds (Plg)	85.8	0.6	13.6
AH-68A-C1	Grd	*	90.6	0.4	9.1
AH-68A-C1	Grd	*	95.2	0.1	4.7
AH-68A-C4	Grd	*	86.2	0.4	13.4
AH-11-C1	Grd	*	74.6	0.4	25.0
AH-12-C1	Grd	*	93.4	0.5	6.0
AH-12-C1	Grd	*	97.9	0.3	1.8
AH-12-C1	Grd	*	97.3	1.6	1.2
AH-12-C1	Grd	*	69.3	1.1	29.5

D-QD = Diorite – Quartz diorite Grd = Granodiorite

Table 5. Th–U concentrations (ppm) and U–Pb ages of zircons from the rock-forming of the Ariz pluton: diorite (AH-105 sample), quartz diorite (AH-108 sample), and granodiorite (AH-11 & AH-12E samples) from the Ariz pluton. Pinkish alkali feldspar granites (AH-13) intruded in the Ariz pluton

Spot	U (ppm)	Th (ppm)	$^{207}\text{Pb}^*/^{235}\text{U}$	$\pm\%$	$^{206}\text{Pb}^*/^{238}\text{U}$	$\pm\%$	err. corr.	$^{206}\text{Pb}/^{238}\text{U}$ Age (Ma)
AH-11-7.1	243	152	0.67	3.1	0.081	3.3	0.86	502 \pm 16
AH-11-8.1	254	186	0.69	3.2	0.085	3.4	0.85	526 \pm 17
AH-11-9.1	105	47	0.69	3.7	0.081	3.6	0.80	503 \pm 17
AH-11-10.1	120	48	0.64	3.4	0.079	3.3	0.80	488 \pm 16
AH-12E-1.1	227	117	0.70	2.3	0.090	2.4	0.8	556 \pm 13
AH-12E-3.1	136	58	0.68	2.6	0.087	2.6	0.8	537 \pm 14
AH-12E-4.1	105	57	0.66	2.2	0.088	1.9	0.6	543 \pm 10
AH-12E-5.1	154	66	0.72	2.0	0.095	1.8	0.7	584 \pm 10
AH-12E-7.1	71	23	0.75	9.4	0.094	4.2	0.4	577 \pm 23
AH-12E-8.1	197	100	0.69	1.9	0.085	1.8	0.7	527 \pm 9
AH-12E-9.1	57	27	0.73	2.5	0.088	2.0	0.6	545 \pm 10
AH-12E-11.1	169	94	0.67	3.2	0.087	2.4	0.7	538 \pm 12
AH-12E-15.1	168	79	0.71	1.9	0.089	1.8	0.7	550 \pm 9
AH-12E-17.1	91	36	0.68	2.6	0.089	2.3	0.7	550 \pm 12
AH-105-1.1	249	127	0.720	1.8	0.0876	1.1	0.47	541 \pm 6
AH-105-3.1	249	121	0.721	2.1	0.0878	1.6	0.59	542 \pm 9
AH-105-4.1	362	190	0.668	1.9	0.0846	1.6	0.61	523 \pm 8
AH-105-5.1	400	226	0.696	1.5	0.0856	1.0	0.51	529 \pm 5
AH-105-6.1	258	123	0.676	1.8	0.0867	1.1	0.47	536 \pm 6
AH-108-6.1	84	39	0.70	2.2	0.090	1.9	0.6	554 \pm 10
AH-108-9.1	170	99	0.69	2.2	0.085	1.8	0.6	528 \pm 9
AH-108-7.1	921	309	0.71	4.5	0.092	4.1	0.6	568 \pm 22
AH-108-11.1	186	109	0.72	2.0	0.088	1.8	0.7	544 \pm 10
AH-108-12.1	87	36	0.63	4.1	0.083	2.7	0.5	512 \pm 13
AH-108-15.1	57	22	0.68	3.2	0.088	2.9	0.7	542 \pm 15
AH-13-4.1	273	150	0.644	1.9	0.0835	1.1	0.45	517 \pm 5
AH-13-5.1	179	111	0.675	2.6	0.0853	1.2	0.45	528 \pm 6
AH-13-6.1	171	99	0.694	2.2	0.0879	1.2	0.44	543 \pm 6
AH-13-7.1	201	129	0.703	2.2	0.0882	1.2	0.45	545 \pm 6
AH-13-8.1	147	64	0.717	2.3	0.0872	1.4	0.48	539 \pm 7
AH-13-11.1	162	82	0.644	2.3	0.0854	1.2	0.43	528 \pm 6
AH-13-13.1	182	88	0.712	3.1	0.0863	1.1	0.35	533 \pm 6
AH-13-14.1	103	58	0.694	4.2	0.0868	1.3	0.33	537 \pm 7
AH-13-15.1	235	152	0.684	2.0	0.0858	1.1	0.45	530 \pm 6

Errors are 1-sigma; Pb and Pb* indicate the common and radiogenic portions, respectively.

(1) Common Pb corrected using measured ^{204}Pb .

(2) Common Pb corrected by assuming $^{206}\text{Pb}/^{238}\text{U}$ - $^{207}\text{Pb}/^{235}\text{U}$ age-concordance

(3) Common Pb corrected by assuming $^{206}\text{Pb}/^{238}\text{U}$ - $^{208}\text{Pb}/^{232}\text{Th}$ age-concordance

Mineral Chemistry

Amphibole

Selected electron microprobe analyses of amphiboles from Ariz pluton are presented in Table 2. Based on classification diagrams (Leake et al., 1997 & 2003), analyzed amphiboles belong to calcic amphibole group (Fig. 7a) and are mainly classified as magnesiohornblende, actinolitic

hornblende, and ferro-actinolitic hornblende (Fig. 7b). A small number of amphiboles fall into the compositional range of actinolite, ferro-actinolite, ferro-hornblende, edenite, and siliceous edenite.

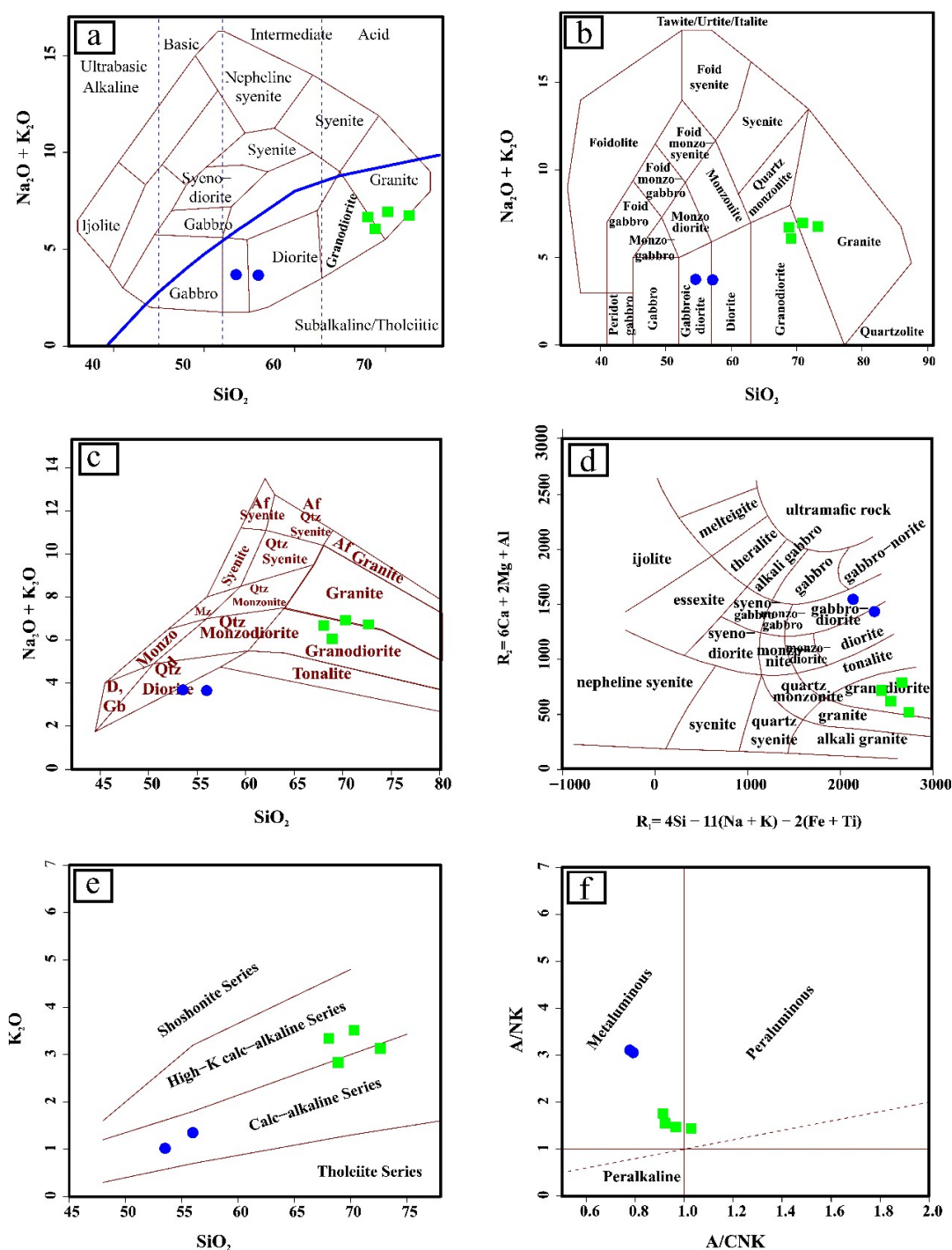


Figure 6. Nomenclature and classification of Ariz pluton rocks. a, b and c) $\text{Na}_2\text{O} + \text{K}_2\text{O}$ vs SiO_2 (Cox et al., 1979; Middlemost, 1985; Middlemost, 1994, respectively), (d) R_1 - R_2 diagram (De La Roche et al., 1980); (e) K_2O vs SiO_2 (Peccerillo & Taylor, 1976); and (f) $\text{Al}_2\text{O}_3/(\text{Na}_2\text{O} + \text{K}_2\text{O}) - \text{Al}_2\text{O}_3/(\text{CaO} + \text{Na}_2\text{O} + \text{K}_2\text{O})$ (Shand, 1943)

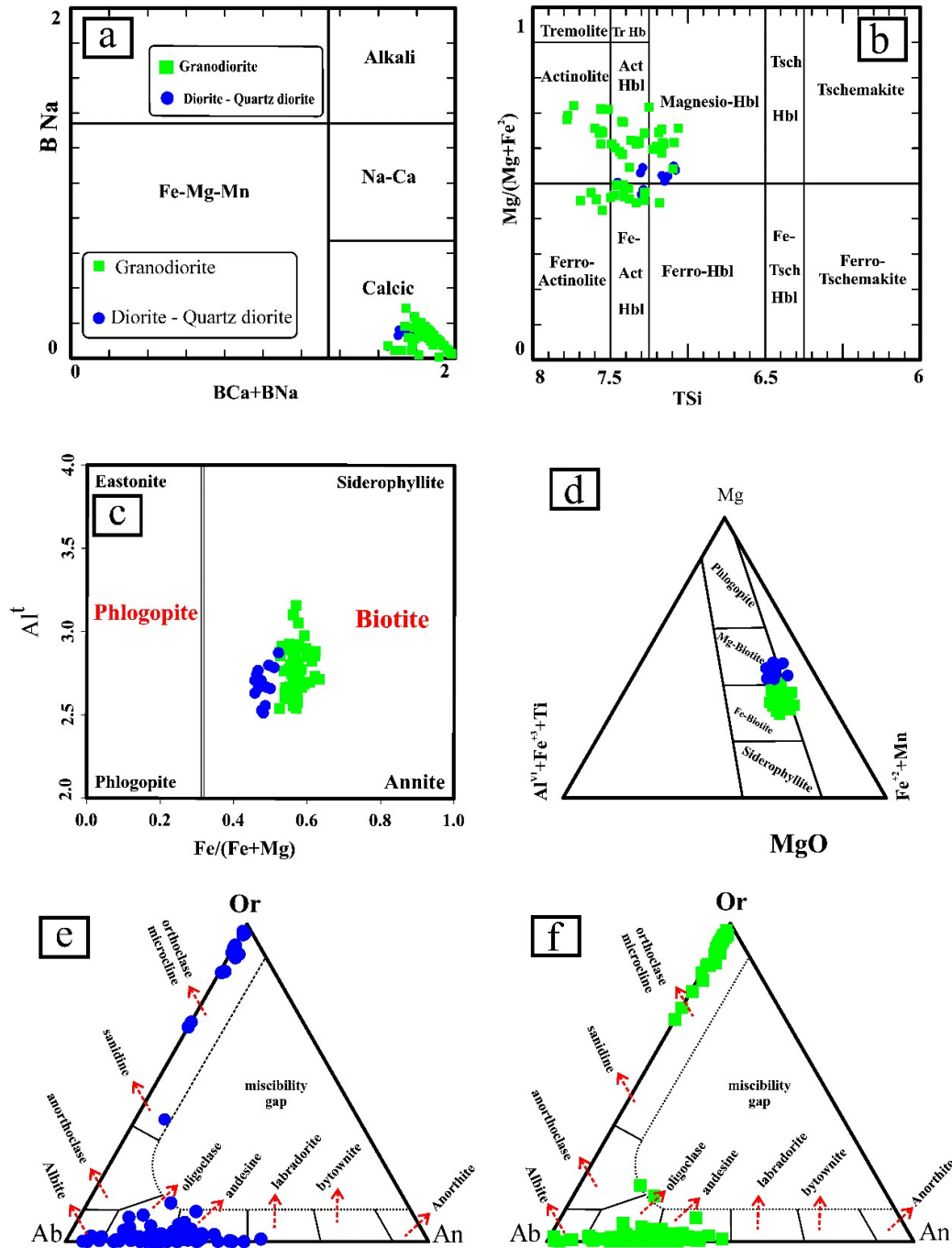


Figure 7. (a) BNa vs Fe/(Fe+Mg) and (b) Mg/(Fe²⁺+Mg) (b) for classification of the amphiboles from Ariz pluton (Leake et al., 1997). (c) Al total vs Fe/(Fe+Mg) (Deer et al., 1992) and (d) Mg-Al^{VI}+Fe³⁺+Ti-Fe²⁺+Mn²⁺ ternary plot (Foster, 1960) for the studied micas from the Ariz pluton. Ternary diagrams for feldspars of (e) diorite, quartz diorites, and (f) granodiorites (Deer et al., 1992)

Biotite

Results of the microprobe analysis of biotite are given in Table 3. It is assumed that all the iron in the biotites is in the Fe²⁺ valence state. Based on the Al^T plot vs Fe/(Fe + Mg) (Guidotti, 1984), which distinguishes the micas into four groups: annite, phlogopite, siderophyllite, and eastonite. In this diagram, Fe-Mg and Si-Al cation exchanges between end members are

considered and the ratio $\text{Fe}/(\text{Fe}+\text{Mg}) = 0.33$ separates biotite from phlogopite (Deer et al., 1962 & 2013). All of the studied micas from Ariz pluton fall within the biotite field (Fig. 7c).

The Fe^{2+} , Ti, and Mg contents in biotite influence their color: the higher iron content leads to a deeper brown color in plane-polarized light (Lalonde and Bernard, 1993). The $\text{Fe}/(\text{Fe} + \text{Mg})$ values of biotites are almost uniform and constant at 0.46–0.63, reflecting the oxidation state of the magma and the primary nature of the biotites studied (Xianwu et al., 2009).

Composition of biotites from the Ariz pluton in the $\text{Mg}-\text{Al}^{\text{VI}}+\text{Fe}^{3+}+\text{Ti}-\text{Fe}^{2+}+\text{Mn}^{2+}$ ternary diagram (Foster, 1960) (Fig. 7d) plot in the magnesio and ferro biotites fields. The studied micas from the diorite and quartz diorite mainly fall within the magnesio-biotite field. And also, the micas from the granodiorites fall within the ferro-biotite field (Figure 7d).

The ternary diagram of $\text{MgO}-10*\text{TiO}_2-\text{FeO}^*+\text{MnO}$ was used to distinguish primary biotites from secondary biotites (Nachit et al., 2005; Fig. 8a). Most biotites plot in the field of primary igneous biotites, with MgO ranging from 5.34 to 12.35 wt% and Al_2O_3 from 11.70 to 17.54 wt% (Supplementary Table 3). A small number of biotites are plotted in the re-equilibrated biotite field, which is actually a statistical tendency and there is practically no microscopic evidence to confirm the re-equilibration of biotites.

Based on the cationic and oxide content of major elements in biotites, such as Al^{IV} , Al^{VI} , Al_2O_3 , FeOt, and MgO can be used to determine the magmatic series and tectonic environment of rocks containing biotites. Compositional position of biotites of the Ariz pluton on the $\text{Al}^{\text{IV}} + \text{Al}^{\text{VI}}$ vs Mg diagram (Nachit et al., 1985) is plotted on the subalkaline and calc-alkaline fields (Fig. 8b). Al_2O_3 vs FeOt (total), Al_2O_3 vs FeOt (total), and Al_2O_3 vs MgO diagrams, and also FeOt-MgO- Al_2O_3 ternary plot (Abdel-Rahman, 1994), were used for this purpose (Fig. 8c & d, selected as a candidate). A field corresponds to the non-orogenic alkaline series, C field is associated with calc-alkaline rocks, and P field pertains to peraluminous samples resulting from the melting of continental crust in collisional environments. In all of the mentioned diagrams and ternary plot, the biotites from the Ariz pluton are mainly plotted within the calc-alkaline and subalkaline field, which confirms the results obtained on the basis of whole rock geochemistry (see fig. 8b, c & d).

Feldspars

The feldspars are in the form of medium-grained crystals; their composition is given in Table 4 and shown in Fig. 7e & f. Based on their anorthite content, plagioclases range from andesine to oligoclase, with a few analyses in the albite field. It should be noted that potassium feldspars (orthoclase) are rarely found in diorites and quartz diorites, while granodiorites contain higher amounts of orthoclase. In addition, potassium feldspars are in the range of orthoclase and microcline, which is consistent with microscopic observations and exhibit perthite texture. Overall, total orthoclase content of potassium feldspars in the Ariz pluton ranges between 67% and 97%.

Discussion

Evaluation of crystallization P-T conditions

Amphibole geothermobarometry - Diorites and quartz diorites

Amphibole is one of the most reliable minerals for geothermobarometry in calc-alkaline igneous rocks, as it is found in almost all intermediate to felsic rocks. Several geobarometric calibrations have been proposed to estimate the crystallization temperature and pressure of amphiboles (Anderson and Smith, 1995; Hawthorne et al., 1997; Ridolfi et al., 2010, Ridolfi et al., 2021).

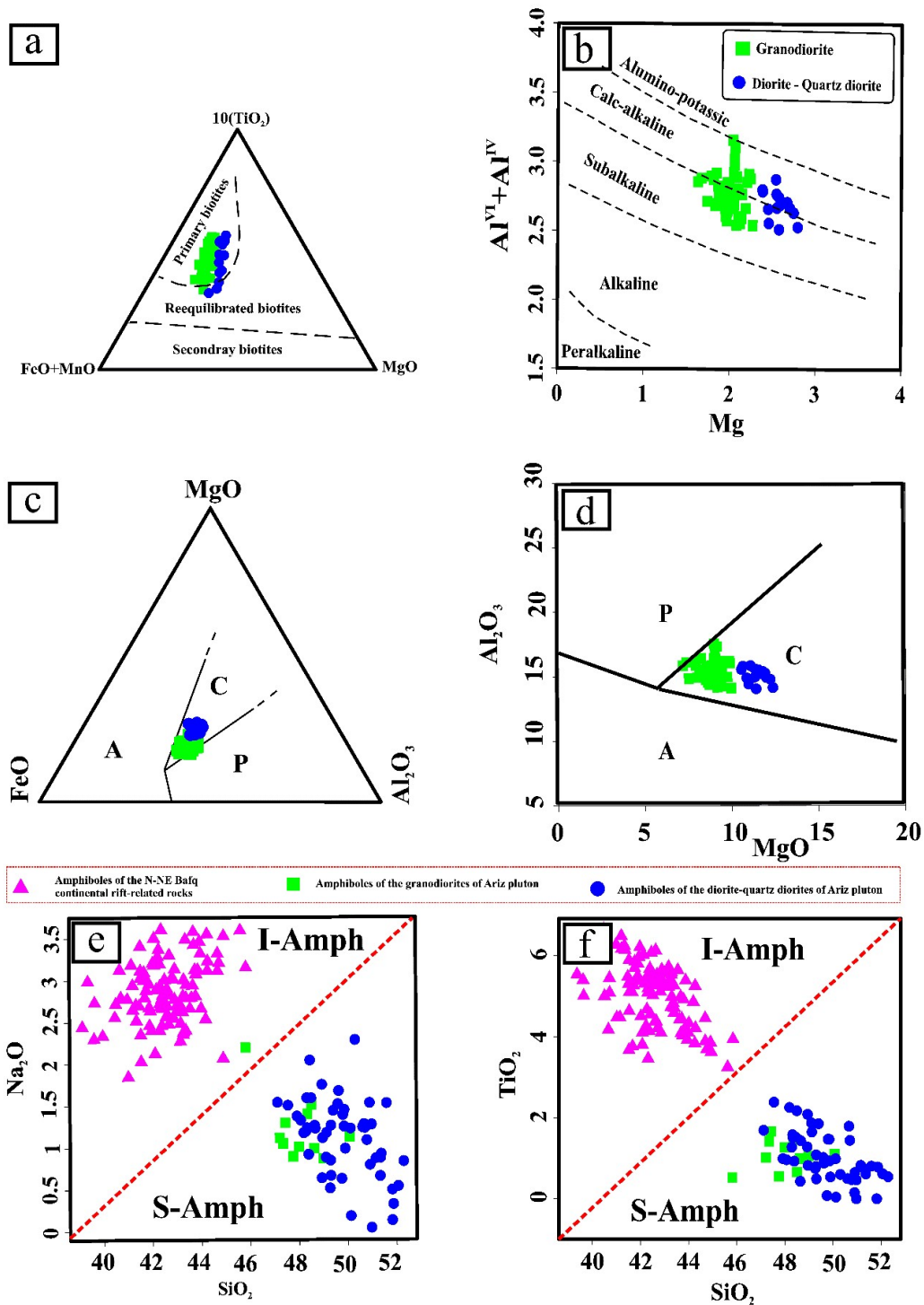


Figure 8. (a) $10*\text{TiO}_2\text{-FeO}^*\text{-MgO}$ (Nachit et al., 2005); (b) Compositional position of biotites of the Ariz pluton on the $\text{Al}^{\text{IV}} + \text{Al}^{\text{VI}}$ vs Mg diagram (Nachit et al., 1985); (c & d) $\text{FeO}^*\text{-MgO-Al}_2\text{O}_3$ and Al_2O_3 vs MgO discriminant ternary plot and diagram for biotites in anorogenic alkaline suites (field A), biotites in peraluminous (including S-type) suites (field P), and biotites in calc-alkaline orogenic suites (field C). Biotites of the Ariz pluton rocks are plotted in the field of calc-alkaline suite. (e & f) Na_2O and TiO_2 vs SiO_2 diagrams for discrimination between amphiboles of intraplate (I-Amph) and suprasubduction (S-Amph) environments (Coltori et al., 2007). Symbols are as follows: blue circles (amphiboles of Ariz diorite and quartz diorites), green square (amphiboles of Ariz granodiorites), purple triangular (amphiboles of N-NE Bafq rift-related rocks)

Amphibole is stable over a wide range of pressures (1–23 kbar) and temperatures (400–1150 °C) (Blundy & Holland, 1990; Stein & Dietl, 2001; Ridolfi, 2021). Several geobarometers have been proposed to calculate pressure based on the Al in hornblende (Hammarstrom & Zen, 1986; Hollister et al., 1987; Johnson and Rutherford, 1989; Anderson and Smith, 1995; Ridolfi et al., 2010, Ridolfi et al., 2021). In addition, the amount of aluminum in hornblende is also temperature sensitive control. In this study, geobarometer based on the Al content of hornblende (Putirka, 2016) is used to estimate the pressure prevailing during the crystallization of amphiboles. With increasing pressure and temperature, the amount of aluminum in hornblende increases notably. The average Al_2O_3 content in the analyzed hornblendes ranges between 4.68 and 6.68 wt%, indicating that they crystallized at pressures of 2.8 to 1.3 kbar (Table 2, Fig. 9). The crystallization temperature of diorites and quartz diorites was calculated to be between 861 and 713 °C using a thermometer based on the amount of aluminum present in the hornblende (Equation 5, Putirka, 2016, Fig. 9).

Amphibole geothermobarometry- Granodiorites

In order to estimate the pressure of amphibole crystallization in granodiorites of the Ariz pluton, the Al in hornblende geobarometer was applied (Mutch et al., 2016). The Al content of hornblende increases significantly with increasing temperature and pressure. The Al_2O_3 content in the analyzed amphiboles ranges between 5.96 and 8.52 wt%, indicating that they crystallized at pressures of 2.8 to 2 kbar (Table 2, Fig. 9). Based on experimental data from coexisting amphibole-melt (liquid) equilibrium, Putirka (2016) proposed the following equation to determine the crystallization temperature of amphiboles.

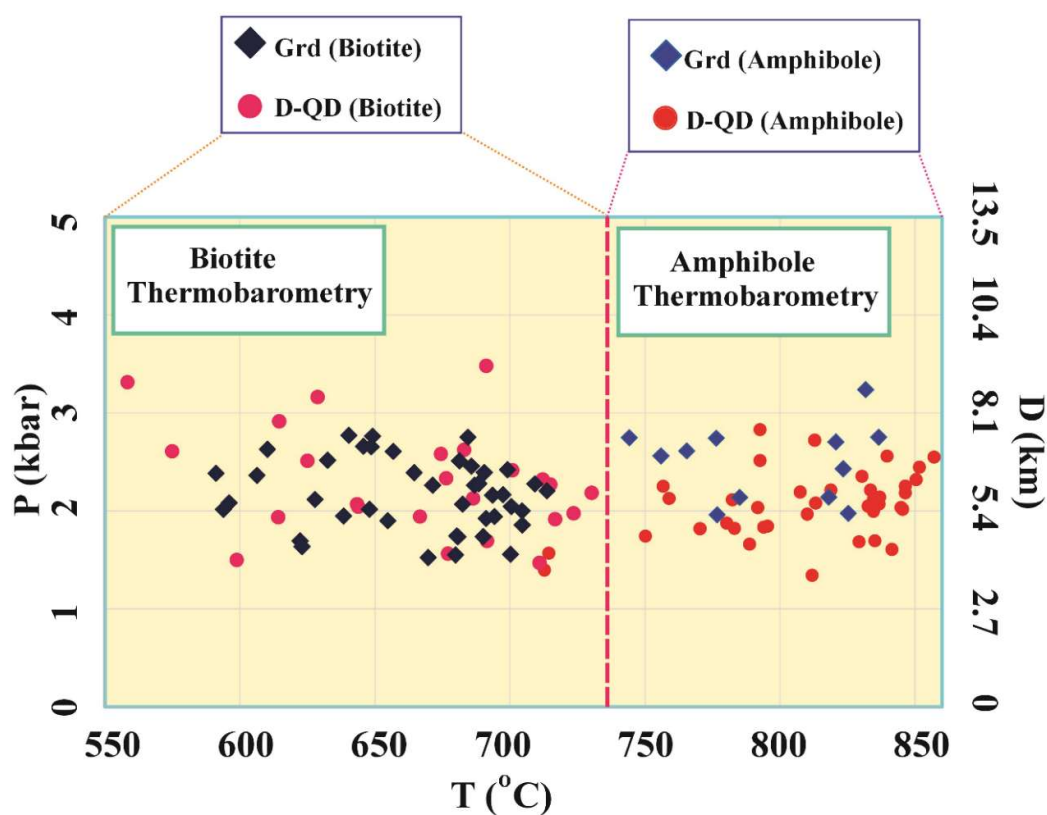


Figure 9. P-T conditions of crystallization or closure of the rocks forming the Ariz pluton based on the mineral chemistry of hornblende and biotite (see text for further explanations). D-QD = diorite – quartz diorite, Grd = granodiorite, D = Depth (km)

$$T(^{\circ}\text{C}) = 1201.4 - 97.93[\text{Si}_{\text{Amp}}] + 201.82[\text{Ti}_{\text{Amp}}] + 72.85[\text{Mg}_{\text{Amp}}] + 88.9[\text{Na}_{\text{Amp}}] + 40.65[\text{P}(\text{GPa})]$$

Meanwhile, according to another equation from (Putirka, 2016) (Equation No. 1), temperatures of 837 to 744 °C have been obtained for the crystallization of Ariz granodiorites (Table 2, Fig. 9).

Biotite geothermobarometry

Biotite is an important indicator of the geochemical evolution of the parent magma (Ashrafi et al., 2024). The abundance of biotite in Ariz granodiorites indicates hydrous magma origin, as biotite typically contains up to 5% volatile compounds (including OH, F, and Cl) (Table 3; Fig. 9). As mentioned previously, the analyzed biotites plot within the primary igneous field on $10 \times \text{TiO}_2\text{-FeO-MgO}$ diagram (Fig. 5a, Nachit et al., 2005). Titanium content in biotite is known to correlate positively with temperature making it suitable for geothermometry.

According to the empirical thermometer proposed by Henry et al. (2005), crystallization temperatures for the biotites in granodiorites were estimated 712 ± 12 °C and 606 °C. Furthermore, there is a positive correlation between the Al^{T} content of biotite and the crystallization pressure. Based on the barometric equation of Uchida et al. (2007):

$$P(\text{kbar}) = 3.03 \times \text{Al}^{\text{T}} - 6.53(\pm 0.33)$$

where Al^{T} is the total number of aluminum cations per 22 oxygens, pressures for the Ariz granodiorite biotites were calculated between 3.12 ± 0.33 and 2.1 kbar (Fig. 9). These results are consistent with the amphibole pressure estimates obtained using the Mutch et al. (2016) barometer (Table 2). All geothermobarometric results are summarized and illustrated in the P–T diagram (Fig. 9), confirming that the Ariz granodiorite crystallized under shallow crustal conditions in the range of ~2–3 kbar and 600–850 °C.

U-Pb zircon geochronology

Zircons were isolated from five samples, such as follows: AH-105 (diorite), AH-108 (quartz diorite), AH-11 & AH-12E (granodiorite), and AH-13 (pink alkali feldspar granite). It should be noted that pink alkali feldspar granite intruded into the dioritic rocks of Ariz Pluton. Zircons are generally small, transparent, and rectangular, exhibiting relatively uniform morphology (Fig. 10). Grain sizes range between 50 to 280 μm , with aspect ratios (length to width) varying from 0.1 to 1.3. Cathodoluminescence imaging reveals distinct zoning. The isotopic analyses results of these zircons (Table 5) yielded ages that were plotted on Concordia diagrams, with the results summarized as follows:

Error-weighted	$^{206}\text{Pb}/^{238}\text{U}$ ages (Ma.)	Sample No.	Lithology
MSWD = 2.1	532 ± 5	AH-13	Alkali feldspar granite
MSWD = 1.8	520 ± 12	AH-11	Granodiorite
MSWD = 2.5	551 ± 11	AH-12 E	Granodiorite
MSWD = 3.0	533 ± 9	AH-108	Quartz diorite
MSWD = 1.8	534 ± 14	AH-105	Diorite

Cathodoluminescence images and U-Pb Concordia diagrams of zircons from selected samples of the Ariz pluton are presented in Figs. 10 and 11. The results confirm that Ariz pluton crystallized during the Late Neoproterozoic (Ediacaran)-Lower Cambrian. Field evidence, such as the intrusion of granodiorites into diorites and quartz diorites, as well as the presence of microgranular mafic enclaves and mafic accumulations rich in amphibole (green hornblende) and biotite (Figs. 4b to f and 5e & f), indicates that granodiorites are younger than diorites and quartz diorites and represent a later magmatic event.

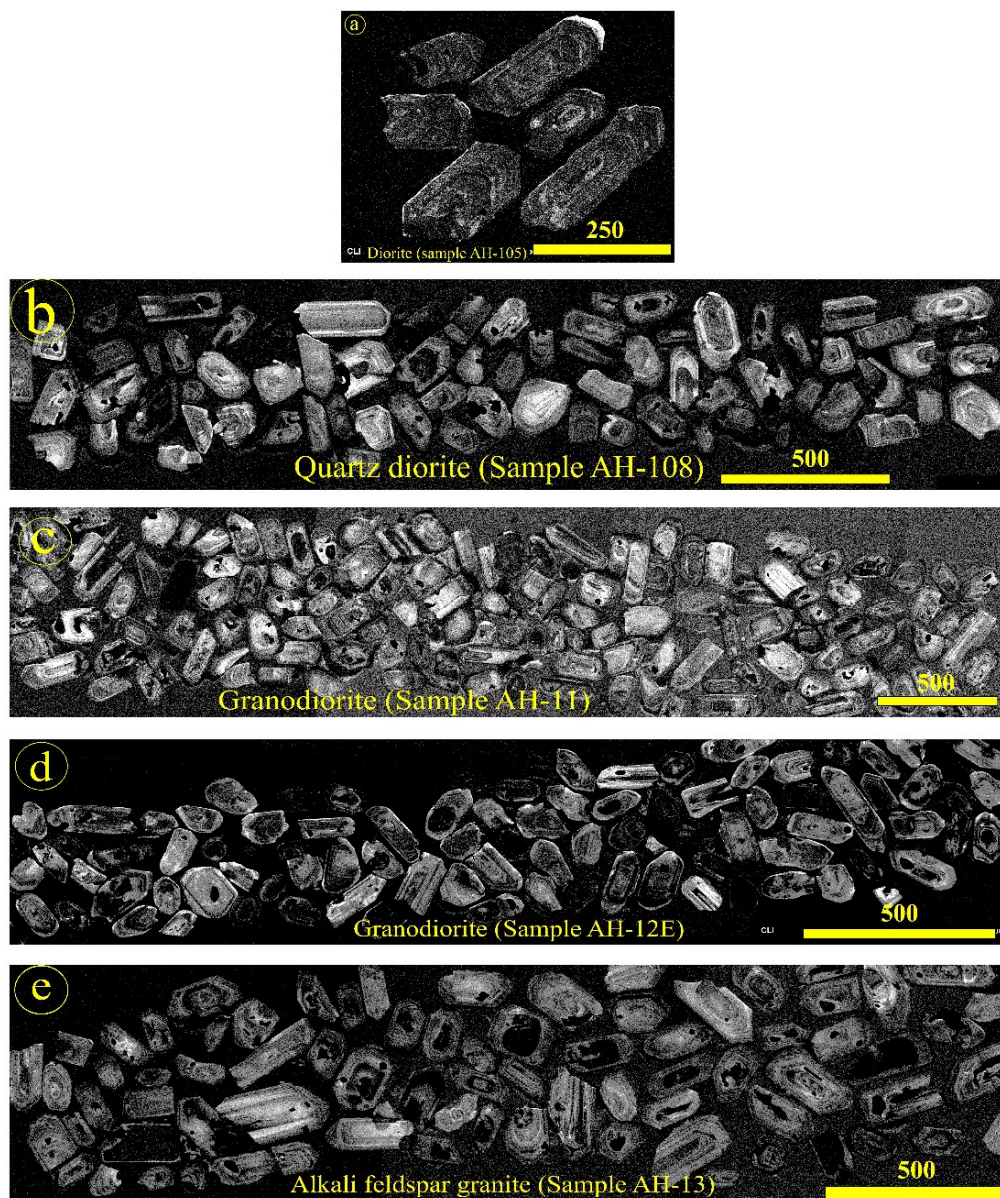


Figure 10. CL images of zircons separated from the studied rocks of Ariz pluton for zircon U-Pb dating. Linear scales are in terms of μm . (a) Diorite, (b) Quartz diorite, (c & d) Granodiorite, and (e) Alkali feldspar granite. It should be noted that alkali feldspar granites cut Ariz pluton in the form of plugs or small-scale intrusions

Granodiorites contain higher amounts of biotite and potassium feldspar than diorites and quartz diorites, suggesting greater crustal contamination during their evolution. This is further supported by the presence of inherited zircon grains, with ages ranging from ~ 600 to 1000 Ma, which are evident in the Concordia diagram of the AH-12E sample. Sample AH-108 also displays inherited zircons, suggesting the same evolution for the diorites and quartz diorites. In contrast, the pink alkali feldspar granites, which intrude in all previous units as small-scale apophyses or dikes, yields a younger age of 532 ± 5 Ma, marking the final stage of the magmatic episode. Obtaining more dating results from these types of rocks will help in better understanding of the geological past of Iran.

Notably, previous U-Pb dating (Ramezani and Tucker, 2003) on sample G54 from the granodiorite part of the Ariz pluton yielded an age of 533 ± 1 Ma, supporting the age range

obtained in this study. Together, these data suggest that Ariz pluton crystallized between 535 and 530 Ma, during the Early Cambrian. Considering the geological history of the Posht-e-Badam block and the ages of the inherited zircon grains, it is safer or more reliable to assume that Ariz pluton is the product of Late Neoproterozoic - Early Cambrian magmatic activity, related to regional crustal melting and crystallization processes.

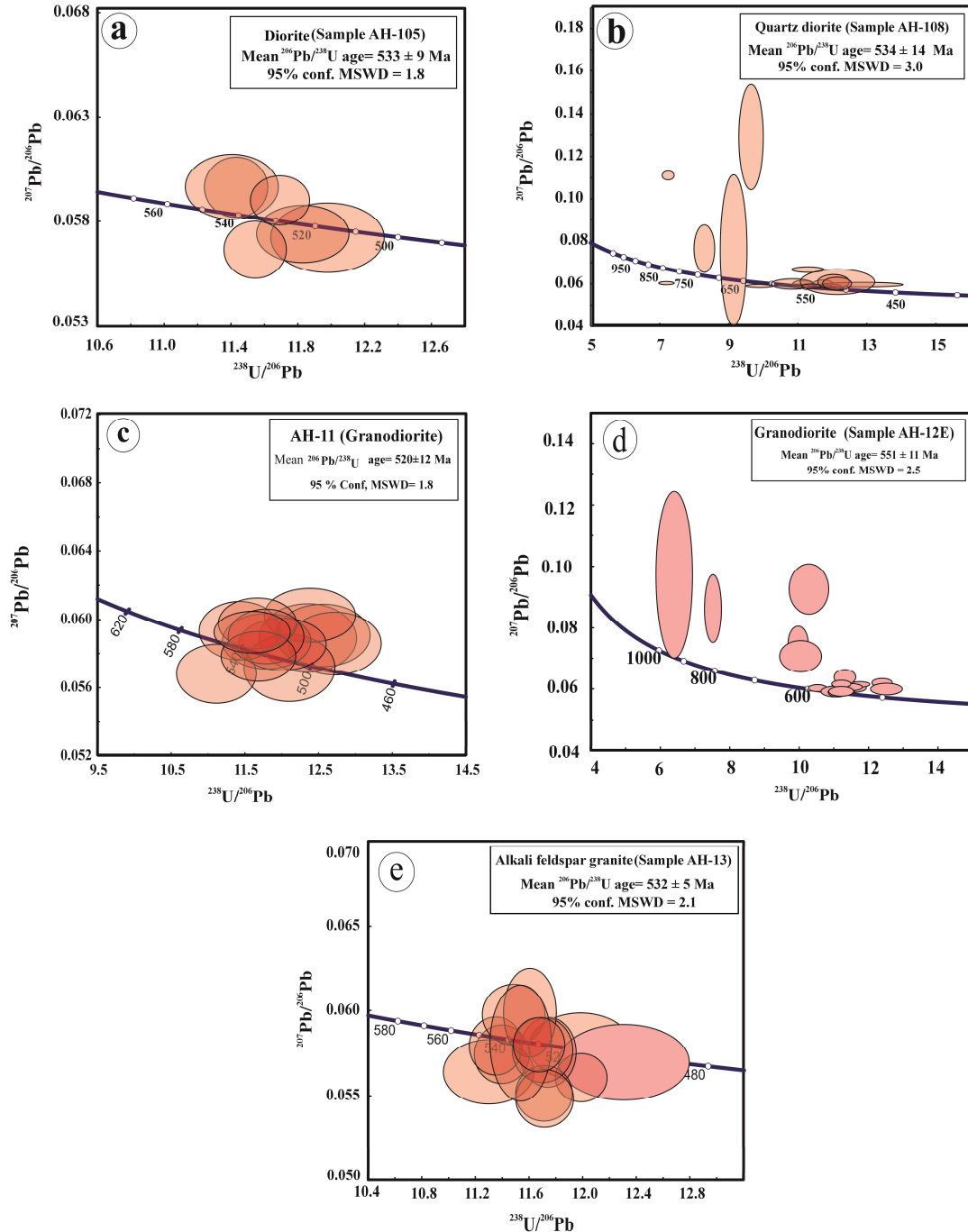


Figure 11. Concordia diagrams for zircons that were separated from the studied rocks of Ariz pluton for zircon U-Pb dating. Scale in terms of μm . (a) Diorite, (b) Quartz diorite, (c & d) Granodiorite, and (e) Alkali feldspar granite. It should be noted that alkali feldspar granites cut Ariz pluton in the form of plugs or small-scale intrusions

Magmatic nature, tectonic setting, and emplacement model of the Ariz pluton

Biotite is an important ferromagnesian mineral in felsic and intermediate igneous rocks and is indicative of the nature of magmas. All biotites from the Ariz pluton are primary in origin (Fig. 8a), making them reliable indicators of the nature of the parental magma. Biotite crystallizes in a range of magmatic settings, including alkaline anorogenic suites, calc-alkaline orogenic suites, and peraluminous (S-type) suites, but also defines three distinct compositionally defined fields. Biotites from non-orogenic alkaline granites have an average FeO^*/MgO ratio of 7.04, while biotites from orogenic calc-alkaline granites are richer in magnesium and have an average FeO^*/MgO ratio of 1.76 (Abdel-Rahman, 1994; see Figs. 7c & d; and 8b to d). Biotites of peraluminous suites (including S-type granites) have a siderophilic composition and an average FeO^*/MgO ratio of 3.48. In the $\text{Al}^{\text{IV}} + \text{Al}^{\text{VI}}$ vs Mg diagram (Nachit et al., 1985, Fig. 8b), biotites of the Ariz pluton have FeO^*/MgO ratios between 1.50 to 3.07 and are mainly plotted in the field of calc-alkaline orogenic granites (Fig. 8c & d). The inferred orogeny during this Late Neoproterozoic – Early Cambrian period of time, is the Cadomian orogeny that occurred on the northern margin of the Gondwana supercontinent.

Chondrite-normalized rare earth element patterns (REE) (Nakamura, 1984, Fig. 12a) and the mantle-normalized spider diagram (Sun & McDonough, 1989; Fig. 12b) indicate that diorites and quartz diorites are more differentiated than granodiorites. The significant enrichment of granodiorites in light rare earth elements (LREEs) confirms this. This enrichment corresponds with greater abundance of biotite and zircon, both of which can contain LREEs, especially biotite. All samples show significant Pb enrichment, suggesting crustal contamination during magma evolution. The observed negative anomalies in Nb, Ti, Ta, alongside the positive anomalies of Pb, Sr and the relative enrichment of LILE and LREE over HREE and HFSE, are characteristic of rocks formed in subduction-related, active continental margin environments (Pearce, 1983; Wilson, 1989; Winter, 2010). Overall, these geochemical diagrams suggest that Ariz pluton was formed by processes such as fractional crystallization, crustal assimilation, and magma contamination, although further geochemical investigation would be needed to fully determine magma evolution. However, due to financial constraints, further analysis was not possible during this study.

Whole rock geochemical diagrams further constrain the tectonomagmatic setting of the Ariz pluton. Tectonic discrimination diagrams using Nb-Y, Ta-Yb, Rb-Ta+Yb, and Rb-Y+Nb (Pearce et al., 1984) also place most samples within the VAG field (Fig. 12c, for example). Similarly, on the Rb/30-Hf-Ta*3 ternary diagram (Harris et al. 1986, Fig. 12d), the samples from Ariz pluton fall within the field of volcanic arc granites (VAG). Additionally, the Th/Ta vs Ta/Yb, Th/Hf vs Ta/Hf, Th/Ta vs Yb, and Th vs Ta diagrams (Gorton & Schandl, 2000; Schandl & Gorton, 2002), further support that the rocks of Ariz pluton are consistent with an active continental margin setting or province. The Th vs Ta diagram (Schandl & Gorton, 2002), as a representative, is given in Fig. 12e, and indicates an active continental margin setting for the Ariz pluton. Concerning, Th/Yb vs Nb/Yb diagram (Pearce and Peate, 1995 & Qiu et al., 2014; Fig. 12f), samples of the Ariz pluton are plotted in the fields of continental arcs.

One of the approaches to determining geological settings and differentiating subduction environments from intraplate environments involves analyzing the mineral chemistry of amphiboles. S-Amph represents a suprasubduction environment, whereas I-Amph represents a large range of continental and oceanic settings. Suprasubduction environments are characterized by metasomatizing agents with higher degrees of SiO_2 -saturation and lower TiO_2 contents with respect to their counterpart in intraplate settings, but S-Amph is characterized by the lowest Nb contents. Typically, amphiboles originating from intraplate environments have higher TiO_2 and Na_2O contents compared to those from subduction or suprasubduction environments (Coltorti et al., 2007). Ariz pluton amphiboles occupy a completely individual or

separate field with lower Na_2O and more SiO_2 contents, which are typical characteristics of S-Amph or amphiboles of a suprasubduction environment (Fig. 8e & f). Also, for simultaneous comparison, the chemical composition of typical rift-related early Cambrian gabbro, monzogabbro, monzodiorites and diorites of the north-northeast Bafq are plotted on the mentioned diagrams (Fig. 8e & f). All of the amphiboles of Bafq rift-related rocks, clearly plotted in the intraplate field. It should be noted that microprobe results of rift-related rocks of N-NE Bafq magmatic rocks were adopted from Zolala et al. (2025b).

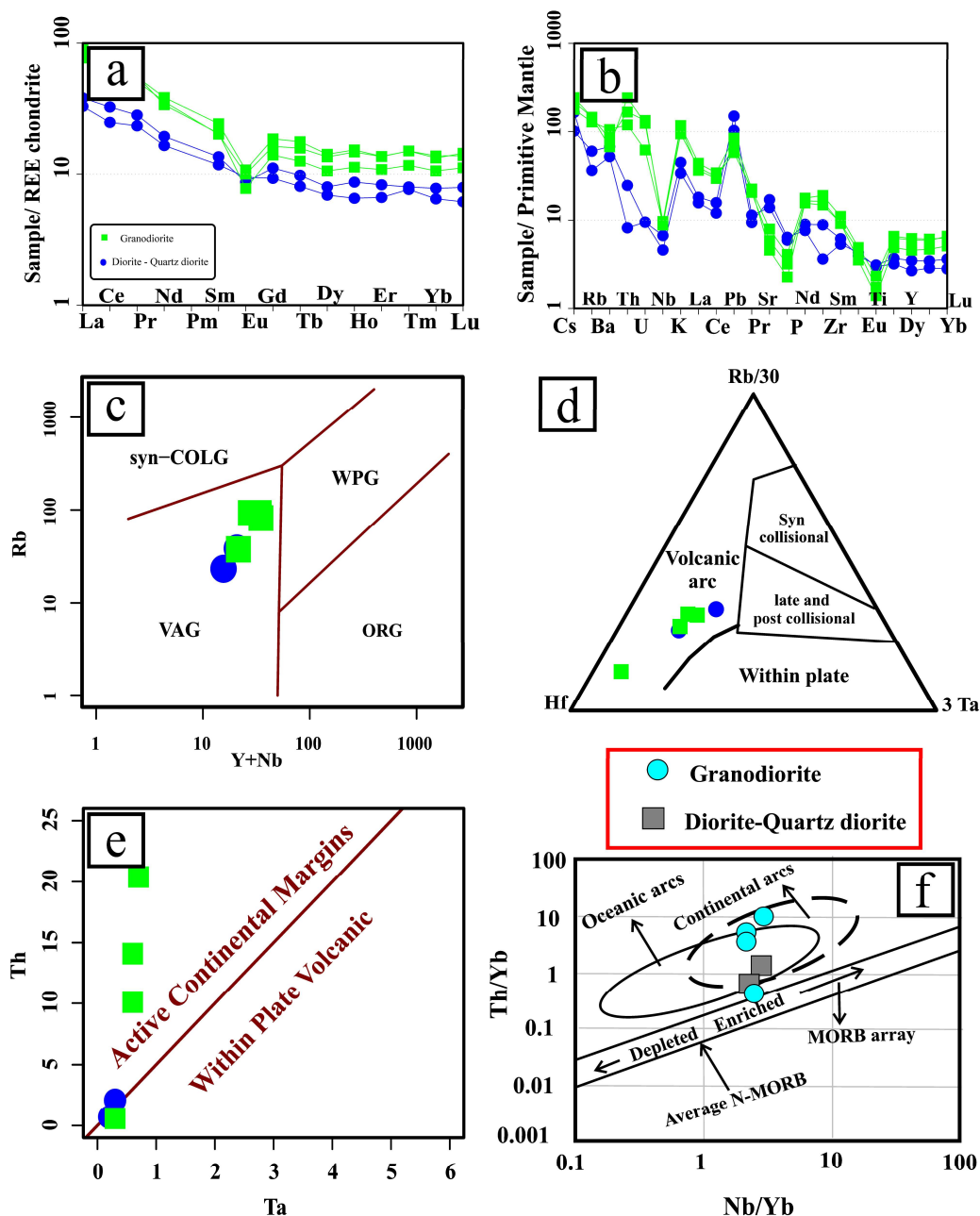


Figure 12. a) Normalized chondrite values of rare earth element patterns (Nakamura, 1974) and b) normalized mantle values spider diagram (Sun and McDonough, 1989) of the Ariz pluton rock units. (c) Rb vs Y+Nb diagrams (Pearce et al. 1984). (d) Hf-Rb/30–3*Ta ternary plot (Harris et al. 1986). (e) Discriminant diagrams for tectonic setting of the Ariz pluton ((Th vs Ta (Schandl & Gorton, 2002); & Th/Yb vs Nb/Yb (Pearce & Peate, 1995 & Qiu et al., 2014))

Similarly, the other major elements oxides such as FeO, MgO, Al₂O₃, TiO₂, CaO, and K₂O vs SiO₂ of Ariz pluton and rift-related rocks of N-NE Bafq, and also amphiboles of the Ariz pluton show the same behavior (not presented in this paper). Therefore, with high confidence, it can be said that Ariz pluton was generated in a subduction zone in the Late Neoproterozoic – early Cambrian period of time. On the other hand, magma generation procedures of the Ariz pluton are part of subduction-related magmatism in the frame of the Cadomian orogeny. The Cadomian orogeny reflects *S*-directed subduction on the northern margin of Greater Gondwana in Ediacaran – Cambrian time (~600-500 Ma). It is well known from the eastern seaboard of North America, western and southern Europe, Turkey and Iran, but is rarely identified in what was its backarc in N. Africa and Arabia (Stern, 2024).

Adakite covers a range of arc rocks ranging from primary slab melt, to slab melt hybridized by peridotite, to melt derived from peridotite metasomatized by slab melt. Adakites can occur in arc settings where unusual tectonic conditions can lower the solidi of even older slabs and their source also includes subducted sediments (Drummond and Defant, 1990; Drummond et al., 1996; Castillo, 2012). Adakites show the following geochemical and isotopic characteristics: SiO₂ ≥56 wt percent, Al₂O₃ ≥15 wt percent, MgO normally <3 wt percent, Mg number ≈0.5, Sr ≥400 ppm, Y ≤18 ppm, Yb ≤1.9 ppm, Ni ≥20 ppm, Cr ≥30 ppm, Sr/Y ≥20, La/Yb ≥20, and ⁸⁷Sr/⁸⁶Sr ≤0.7045 (Richards & Kerrich, 2007; Rezaei-Kahkhaei et al., 2022).

Adakitic rocks are produced through melting of the lower crust or ponded basaltic magma, high-pressure crystal fractionation of basaltic magma and low-pressure crystal fractionation of water-rich basaltic magma plus magma mixing processes in both arc or non-arc tectonic environments (Castillo, 2012). Also, rocks with such compositions have been interpreted to be the products of hybridization of felsic partial melts from subducting oceanic crust with the peridotitic mantle wedge during ascent and are not primary magmas. Comparison of the typical geochemical features of adakites and the rock-forming of Ariz pluton (Fig. 13, and Table 6) indicates that they do not show adakitic features and mostly tend to plot in the field of normal arc andesite, dacite and rhyolite (ADR). Key adakitic geochemical signatures, such as low Y and Yb concentrations and high Sr/Y and La/Yb ratios, can be generated in normal asthenosphere-derived tholeiitic to calc-alkaline arc magmas by common upper plate crustal interaction and crystal fractionation processes and do not require slab melting (Richards & Kerrich, 2007). Common upper plate magmatic processes such as melting-assimilation-storage-homogenization (MASH) and assimilation-fractional-crystallization (AFC) affecting normal arc magmas can be demonstrated to explain the distinctive compositions of most adakite-like arc rocks.

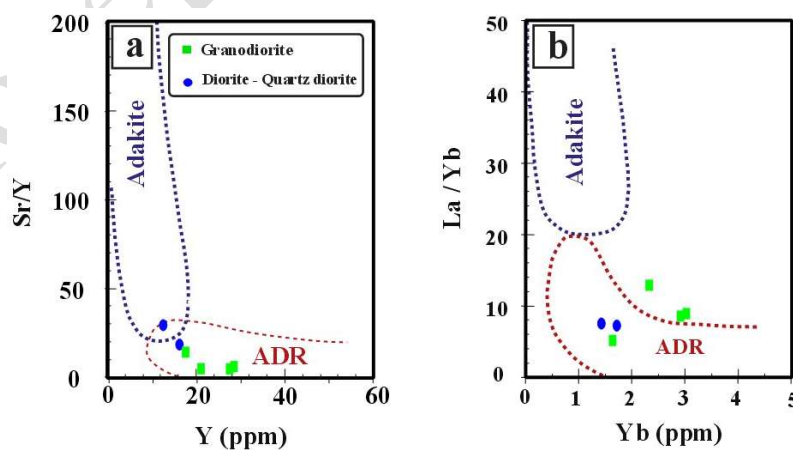


Figure 13. Plots of (a) Sr/Y vs. Y and (b) La/Yb vs. Yb (Castillo, 2012; modified after Drummond and Defant, 1990) that are typically used to distinguish adakite from normal arc andesite, dacite and rhyolite (ADR) lavas. Boundaries used are those more recently proposed by Richards and Kerrich (2007). Most of the Ariz samples are plotted in the ADR field

Table 6. Comparison of the Ariz pluton features with adakites (Castillo, 2012)

	Ariz Pluton (Average for six samples)	Yes/No (*/#)	Features (Castillo, 2012)		Possible link to melting of subducted oceanic basalt
SiO₂	64.9	*	≥ 56 wt. %	High SiO ₂	High-P partial melting of eclogite or amphibolite
Al₂O₃	14.9	*	≥ 15 wt. %	High Al ₂ O ₃	At 70 wt% SiO ₂ ; high P partial melting of eclogite or amphibolite
MgO	2.3	*	<~3 wt. %	Low MgO	Plus low Ni, Cr; if primary melt, not derived from mantle peridotite
Na₂O	3.1	*	>~3 wt. %	High Na ₂ O	High-P partial melting of eclogite or amphibolite
Sr	214.4	#	>~300 ppm	High Sr	Melting of plagioclase or absence of plagioclase in the residue
Y	20.4	#	<~10 ppm	Low Y	Indicative of garnet, hornblende and clinopyroxene in the source
Sr/Y	12.8	#	>~20	High Sr/Y	Indicative of garnet, hornblende and clinopyroxene in the source
Yb	2.2	#	<~1 ppm	Low Yb	Meaning low heavy-REE content; indicative of garnet in the source
La/Yb	8.4	#	>~20	High La/Yb	Enrichment of light-REE/heavy-REE; indicative of garnet in the source
Low HFSE's (Nb, Ta)	5.8	*	nd.	Nb+Ta	As in most arc lavas; Ti-phase or hornblende in the source
low ⁸⁷Sr/⁸⁶Sr	?	?	< 0.704		Plus low ²⁰⁶ Pb/ ²⁰⁴ Pb, K/La, Rb/La, Ba/La and high ¹⁴³ Nd/ ¹⁴⁴ Nd; Normal mid-ocean ridge basalt (MORB) signature
		*	TRUE/Yes		
		#	FALSE/No	nd.	Not exactly determined

Considering these observations, Ariz intrusive body is most likely the product of differential crystallization of magmas that were formed from partial melting of the subducted Proto-Tethys oceanic crust beneath the northern margin of Gondwana during the late Neoproterozoic, or its above modified mantle wedge. These magmas ascended and emplaced in at least two main stages into the upper continental crust or the fore-arc part of the subduction zone. This emplacement occurred at relatively shallow depths, ranging from 8.5 to 4 kilometers. This interpretation is supported by the age data reported for similar igneous bodies in Posht-e-Badam Block, with volcanic arc granite older than 530 Ma (Ghazi et al., 2020). In addition to the Ariz pluton, these types of rocks are exposed in other parts of the Posht-e-Badam Block, including east of the Chadormalu Iron mine or Iron deposit and west of the Posht -e-Badam metamorphic complex. Metamorphosed remnants of the subducted Proto-Tethys oceanic crust, including ophiolites and amphibolites, have been found west of Posht-e-Badam village and east of Saghand (garnet amphibolites in the mining area of the Gelmandeh iron deposit). These complexes are also depicted, albeit exaggeratedly on the 1:100,000 geological maps of Saghand and Robat-e-Posht-e-Badam. In addition, exposures of tectonic mélanges, comprising igneous and metamorphic units, are found along fault boundaries in the region. These rock types have also been documented in central and northwestern Iran (Ghorbani, 2007, 2013, 2021; and Keyghobadi 2016), and southwest of Arousan-e-Khur and Biabanak, along with the Jandaq and Anarak metamorphic complexes. Ophiolitic remnants in these regions include harzburgites, serpentinized dunites, leucogabbros and rodingites (Balouchi, 2019; Ghorbani, 2007). Similar lithologies have also been reported in the Khoy-Takab area in northwest Iran, around the Zarshuran gold mine (Ramezani and Tucker, 2003). This scenario, schematically illustrated in Fig. 14.

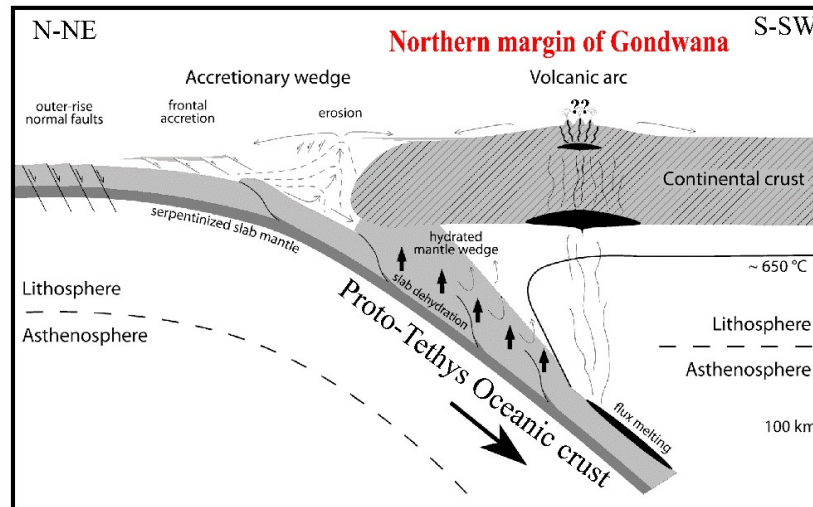


Figure 14. Schematic model for Ariz pluton tectonic setting and magma generation (modified from Ruh et al., 2015)

However, it should be noted that with considering magmatic and metamorphic events from the late Neoproterozoic up to early Cambrian, and U-Pb dating on zircons separated from early-middle Cambrian Lalun Formation (with mainly reddish-brown sandstone composition) (Zoleikhaei et al., 2021, 2023, 2024 & 2025), looks like, the mentioned subduction had not long-lived and could not develop up to produce extensive volcanism, in the northern Gondwana active continental margin. In this relation, pioneering research of Zoleikhaei et al. (2021, 2023 and 2025) is notable. The U–Pb age and Hf isotopic signatures of detrital zircons in the Lalun Formation point to a source in juvenile Neoproterozoic arc terranes and Proterozoic-Archean basement exposed in the Arabian Shield (Zoleikhaei et al., 2021). Integrating constraints from the sedimentary record with geochemical data from the ca. 600-500 Ma igneous rocks in Iran and Anatolia favors an extensional continental margin setting that may be related to escape tectonics or post-collisional relaxation during Ediacaran–Cambrian following Gondwana assembly (Zoleikhaei et al., 2021).

Conclusion

Ariz pluton comprises diorite, quartz diorite and granodiorite with calc-alkaline geochemical affinity. These rocks have been studied systematically to determine their crystallization conditions, tectonic setting, and to develop the emplacement model of the plutonic complex.

Rocks forming of the Ariz pluton have a calc-alkaline and metaluminous nature. These rocks are enriched in light rare earths and large ion lithophile elements, and also depleted in Nb, Ta, and Ti. They show a typical arc pattern of magmatic rocks.

The Al-in-hornblende geobarometer suggests pressures of 1.3 to 2.8 kbar for the diorite – quartz diorite and 2.0 to 2.8 kbar for granodiorite, with corresponding crystallization temperatures calculated from 713 to 861 °C and 744 to 837°C, respectively.

Biotite, which is more abundant in granodiorites, crystallized under conditions of 606 to 713 °C, and 1.52 to 3.12 ± 0.33 kbar.

New zircon U-Pb dating results indicate that the rocks of Ariz pluton crystallized at 535-550 Ma, during the late Neoproterozoic - early Cambrian.

Amphiboles of the Ariz pluton clearly plot in the suprasubduction field, and their host rocks were generated concerning subduction magmatism.

Whole-rock geochemical signatures and mineral chemistry reveal that the parent magmas of the Ariz pluton probably derived from partial melting of the subducted Proto-Tethys oceanic

crust beneath the northern margin of Gondwana supercontinent, or its above modified mantle wedge, during Cadomian orogeny.

Acknowledgment

We extend our sincere gratitude to: 1- Shahrood University of Technology, vice president of research and technology, for the financial support provided during this study, 2- Professor Papadopoulou Lambrini from department of geology at the Aristotle University of Thessaloniki, particularly for conducting the microprobe analysis, 3- Professor Mingguo Zhai from institute of geology and geophysics, Chinese academy of sciences (IGGCAS), especially, for financial support of the whole rock geochemical analyses, 4- Professor Keewook Yi, Hosun Lee from Geochronology Team, Korea Basic Science Institute, Ochang, Republic of Korea and from Core Research Facility, Pusan National University, Busan, South Korea for isotopic analyses and U-Pb zircon dating. We deeply appreciate their invaluable collaborations. We are grateful to the anonymous reviewers, who critiqued this work. Their meaningful and valuable comments or suggestions resulted in a great improvement of this paper. We would like to thank and appreciate the chief editor of the Geopersia journal, Professor Ali Kananian, technical editor Dr Elham Davtalab, Ms. Nabi Zadeh, and all of the other staff at the Geopersia Journal who kindly helped us during the acceptance of the first manuscript and the later reviewing process of this work.

Conflicts of interest

The authors declare that there are no conflicts of interest regarding the publication of this paper. No financial or personal relationships exist that could have influenced the work reported in this manuscript.

Authors' contributions

Mohsen Hamidi: Conceptualization, Methodology, Software, Formal analysis, Investigation, Resources, Data Curation, Writing - Original Draft.

Mahmood Sadeghian: Conceptualization, Methodology, Software, Validation, Formal analysis, Investigation, Resources, Review & Editing, Supervision, Project administration.

Masood Alipour-asl: Formal analysis, Investigation, Resources, Data Curation, Review & Editing.

Maryam Sheibi: Conceptualization, Methodology, Software, Validation, Formal analysis, Investigation, Resources, Review & Editing, Advise.

Mehdi Rezaei Kahkhaei: Conceptualization, Methodology, Software, Validation, Formal analysis, Investigation, Resources, Review & Editing, Advise.

Lambrini Papadopoulou: Microprobe analysis, Investigation, Resources, Data Curation, Main Funding acquisition.

Zhai Mingguo: Formal analysis, Investigation, Data Curation, Funding acquisition, financial support.

Foteini Aravani: Formal analysis, Data Curation, Review & Editing.

Keewook Yi, Zircon U-Pb Dating and Isotopic Analysis.

Hosun Lee, Hand-pick up zircon grains and Zircon U-Pb Dating

References

Abbott, R. N., Clarke, D. B. 1979. Hypothetical liquidus relationships in the subsystem $\text{Al}_2\text{O}_3\text{-FeO-}$

- MgO projected from quartz, alkali feldspar and plagioclase for a $(H_2O) < \text{or} = 1$. The Canadian Mineralogist, 17(3): 549-560.
- Abdel-Rahman, Abdel-Fattah M. 1994. "Nature of biotites from alkaline, calc-alkaline, and peraluminous magmas." Journal of Petrology 35, no. 2: 525-541.
<https://doi.org/10.1093/petrology/35.2.525>
- Aghanabati, A., 2004. Geology of Iran. Geological survey of Iran.
- Alavi, M., 1991. Sedimentary and structural characteristics of the Paleo-Tethys remnants in northeastern Iran. Geological Society of America Bulletin, 103(8), pp.983-992.
[https://doi.org/10.1130/0016-7606\(1991\)103<0983:SASCOT>2.3.CO;2](https://doi.org/10.1130/0016-7606(1991)103<0983:SASCOT>2.3.CO;2)
- Anderson, J.L., Smith, D.R., 1995. The effects of temperature and fO_2 on the Al-in hornblende barometer. American Mineralogist 80, 549–559.
<https://doi.org/10.2138/am-1995-5-614>
- Asadi S. A. A., 2017. Geochemistry and geochronology of igneous and metamorphic rocks from Neybaz complexes, central Iran, Unpublished M.Sc. Thesis, Damghan University, School of Earth Sciences, 143 pages (in Persian with English abstract).
- Ashrafi, N., Dabiri R., & Jahangiri A., 2024. Some chemical variations in biotite, phlogopite, and muscovite, considering their tectonic setting, Geopersia 2024, 14(2): 307-325. DOI: 10.22059/GEOPE.2024.373882.648749
- Askari N., 2021. Petrology and genesis of Zarrin intrusion, north of Ardekan, Unpublished Ph.D. Thesis, Lorestan University, Faculty of Earth Sciences, Department of Geology, 170 Pages (in Persian with English abstract).
- Askari N., Zarei Sahamieh R., , Omrani J., Emami M.H., Fiannacca P., Vaccaro C., Tassinari C., 2022. Geochemistry and geochronology of Zarrin intrusion, NE Aredekan, Central Iran, Petrology, Volume:12 Issue: 48, 1-30 Pages (in Persian).
<https://www.magiran.com/p2468197>
- Azizi M., 2013. Petrology and geochemistry of Sefid Sang granitoid pluton and its metamorphic host rocks (south of Biarjomand). Unpublished M.Sc. Thesis, Shahrood University of Technology, Faculty of Earth Sciences, 161 pages (In Farsi, with English abstract).
- Bagheri, S. and Stampfli, G.M., 2008. The Anarak, Jandaq and Posht-e-Badam metamorphic complexes in central Iran: new geological data, relationships and tectonic implications. Tectonophysics, 451(1-4), pp.123-155. DOI: 10.1016/j.tecto.2007.11.047
- Einalou, M. B., Sadeghian, M., Zhai, M., Ghasemi, H., & Mohajjel, M., 2014. Zircon U–Pb ages, Hf isotopes and geochemistry of the schists, gneisses and granites in Delbar Metamorphic-Igneous Complex, SE of Shahrood (Iran): implications for Neoproterozoic geodynamic evolutions of Central Iran. Journal of Asian Earth Sciences, 92, 92-124.
 DOI: 10.1016/j.jseaes.2014.06.011
- Balouchi. S., 2019. Petrology, geochemistry and isotope geology of Jandagh-Arusan metamorphic and igneous complex, Ph.D. Thesis, Shahrood University of Technology, faculty of earth sciences, 429 pages (In Farsi or Persian, with English abstract).
- Berberian, M. and King, G.C.P., 1981. Towards a paleogeography and tectonic evolution of Iran. Canadian journal of earth sciences, 18(2), pp.210-265.
<https://doi.org/10.1139/e81-019>
- Blundy, J.D., Holland, T.J., 1990. Calcic amphibole equilibria and a new amphibole-plagioclase geothermometer. Contributions to Mineralogy and Petrology 104, 208–224.
 doi:10.1007/BF00306444
- Coltorti, M., Bonadiman, C., Faccini, B., Grégoire, M., O'Reilly, S.Y. and Powell, W., 2007. Amphiboles from suprasubduction and intraplate lithospheric mantle. Lithos, 99(1-2), pp.68-84.
<https://doi.org/10.1016/j.lithos.2007.05.009>
- Davoudian, A. R., Bendokht, M., Shabanian, N., Azizi, H., Asahara, Y., Neubauer, F., & Genser, J., 2022. Geochronology and geochemistry of the Ediacaran orthogneisses from the north Shahrekord (Sadegh-Abad), Sanandaj-Sirjan Zone: Insights into magmatic evolution of the Iranian basement. Geological Journal, 57(7), 2788-2811.
<https://doi.org/10.1002/gj.4440>
- Deer, W.A., Howie, R.A., Zussman, J., 1962. Rock-forming minerals. Sheet silicates 3. Wiley.
- Deer, W.A., Howie, R.A. and Zussman, J., 2013. An Introduction to the Rock-Forming Minerals. 3rd Edition, Prentice Hall, Harlow.

- De la Roche, H.D., Leterrier, J.T., Grandclaude, P. and Marchal, M., 1980. A classification of volcanic and plutonic rocks using R1R2-diagram and major-element analyses—its relationships with current nomenclature. *Chemical geology*, 29(1-4), pp.183-210.
[https://doi.org/10.1016/0009-2541\(80\)90020-0](https://doi.org/10.1016/0009-2541(80)90020-0)
- Drummond, M.S., Defant, M.J., 1990. A model for trondhjemite-tonalite-dacite genesis and crustal growth via slab melting: Archean to modern comparisons. *Journal of Geophysical Research - Solid Earth* 95, 21503–21521. <https://doi.org/10.1029/JB095iB13p21503>
- Drummond, M.S., Defant, M.J., Kepezhinskas, P.K., 1996. Petrogenesis of slab-derived trondhjemite–tonalite–dacite/adakite magmas. *Earth and Environmental Science Transactions of the Royal Society of Edinburgh* 87, 205–215.
 Doi: <https://doi.org/10.1017/S0263593300006611>
- Erdman, M.E., Lee, C.T.A., Levander, A. and Jiang, H., 2016. Role of arc magmatism and lower crustal foundering in controlling elevation history of the Nevadaplano and Colorado Plateau: A case study of pyroxenitic lower crust from central Arizona, USA. *Earth and Planetary Science Letters*, 439, pp.48-57.
<http://dx.doi.org/10.1016/j.epsl.2016.01.032>
- Esmacili D., 1996. Petrological and geochemical investigation of Doran and Moghanlou igneous plutons (Zanjan and Takab areas), M.Sc. Thesis, University of Tehran, faculty of earth sciences, department of geology, 333 pages (in Persian).
- Foster, M.D., 1960. Interpretation of the composition of trioctahedral mica. U.S. Geological Survey Professional Paper, v. 354-B, pp. 11–48.
- Ghaemi F., and Saidi A., 2006. Geological map of the Chadormalo (Scale 1: 100,000), Geological survey of Iran publication (in English and Persian).
- Ghazi, J.M., Moazzen, M., Rahgoshay, M. and Wilde, S.A., 2020. Zircon U–Pb–Hf isotopes and whole rock geochemistry of magmatic rocks from the Posht-e-Badam Block: A key to tectonomagmatic evolution of Central Iran. *Gondwana Research*, 87, pp.162-187.
 DOI: 10.1016/j.gr.2020.06.010
- Ghorbani, M., 2007. Economic geology of Iran, Mineral and natural resources of Iran, deposits and natural resources, Arian Zamin publication, 1-496 (in Persian).
- Ghorbani, M., 2013. The economic geology of Iran. Mineral deposits and natural resources. Springer, 1-450.
- Ghorbani, M., 2021. The geology of Iran: tectonic, magmatism and metamorphism. Springer Nature. DOI: 10.1007/978-94-007-5625-0
- Gorton, M.P. and Schandl, E.S., 2000. From continents to island arcs: a geochemical index of tectonic setting for arc-related and within-plate felsic to intermediate volcanic rocks. *The Canadian Mineralogist*, 38(5), pp.1065-1073. <https://doi.org/10.2113/gscanmin.38.5.1065>
- Guidotti, C.V., 1984. Micas in metamorphic rocks. In Bailey, S.W. (Ed.), *Micas*. Mineral. Soc. Am., Rev. Mineral., 13:357–468. <https://doi.org/10.1515/9781501508820-014>
- Hammerstrom, J.M. and Zen, E.A., 1986. Aluminum in hornblende: an empirical igneous geobarometer. *American Mineralogist*, 71(11-12), pp.1297-1313.
- Harris, N.B., Pearce, J.A. and Tindle, A.G., 1986. Geochemical characteristics of collision-zone magmatism. Geological Society, London, Special Publications, 19(1), pp.67-81.
<https://doi.org/10.1144/GSL.SP.1986.019.01.04>
- Hassanzadeh, J., Stockli, D. F., Horton, B. K., Axen, G. J., Stockli, L. D., Grove, M., ... & Walker, J. D., 2008. U-Pb zircon geochronology of late Neoproterozoic–Early Cambrian granitoids in Iran: Implications for paleogeography, magmatism, and exhumation history of Iranian basement. *Tectonophysics*, 451(1-4), 71-96. DOI:10.1016/j.tecto.2007.11.062
- Hawthorne, F.C., Kato, A., Kisch, H.J., Krivovichev, V.G., Linthout, K., 1997. Nomenclature of amphiboles; report of the Subcommittee on Amphiboles of the International Mineralogical Association Commission on new minerals and mineral names. *Mineralogical Magazine* 61, 295–321. <https://doi.org/10.1180/minmag.1997.061.405.13>
- Helmy, H.M., Ahmed, A.F., El Mahallawi, M.M. and Ali, S.M., 2004. Pressure, temperature and oxygen fugacity conditions of calc-alkaline granitoids, Eastern Desert of Egypt, and tectonic implications. *Journal of African Earth Sciences*, 38(3), pp.255-268. DOI: 10.1016/j.jafrearsci.2004.01.002
- Hemmati A., 2009. Stratigraphy Setting, petrology and geochemistry of the SW Mayamey granitoid

- plutons. Unpublished M.Sc. Thesis, Shahrood University of Technology, faculty of earth sciences, 153 pages (In Farsi, with English abstract).
- Henry, D.J., Guidotti, C.V., Thomson, J.A., 2005. The Ti-saturation surface for low-to medium pressure metapelitic biotites: Implications for geothermometry and Ti substitution mechanisms. *Journal of American Mineralogist*, 90, 316–328.
<http://dx.doi.org/10.2138/am.2005.1498>
- Hollister, L.S., Grissom, G.C., Peters, E.K., Stowell, H.H., Sisson, V.B., 1987. Confirmation of the empirical correlation of Al in hornblende with pressure of solidification of calc-alkaline plutons. *American Mineralogist* 72, 231–239.
- Hosseini, S. H., Sadeghian, M., Zhai, M., & Ghasemi, H., 2015. Petrology, geochemistry and zircon U–Pb dating of Band-e-Hezar Chah metabasites (NE Iran): Evidence for back-arc magmatism along the northern active margin of Gondwana. *Geochemistry*, 75(2), 207–218. DOI: 10.1016/j.chemer.2015.02.002
- Hushmandzadeh, A., 1969. *Metamorphisme et granitisation du massif Chapedony (Iran Central): These*, Universite Scientifique et Medicale de Grenoble, France, 242p.
- Irvine, T.N. and Baragar, W.R.A., 1971. A guide to the chemical classification of the common volcanic rocks. *Canadian Journal of Earth Sciences*, 8(5), 523–548.
<https://doi.org/10.1139/e71-055>
- Johnson, M.C., Rutherford, M.J., 1989. Experimental calibration of the aluminum-in hornblende geobarometer with application to Long Valley caldera (California) volcanic rocks. *Geology* 17, 837–841.
- Jones, R.H., 1989. Ternary feldspars: Two-feldspar assemblages at P (H₂O) = 5 kbar. *Mineralogical Magazine* 53, 347–355.
[https://doi.org/10.1130/0091-7613\(1989\)017<0837: ECOTAI>2.3.CO;2](https://doi.org/10.1130/0091-7613(1989)017<0837: ECOTAI>2.3.CO;2)
- Karimpour, M. H., Lang Farmer, G., Stern, C. R. and Salati, E., 2011. U-Pb zircon geochronology and Sr-Nd isotopic characteristic of Late Neoproterozoic Bornaward granitoids (Taknar zone exotic block), Iran, *Iranian journal of crystallography and mineralogy*, 19th year, No 1. PP: 1-18.
<http://ijcm.ir/article-1-478-en.html>
- Keyghobadi Limjiri, F., 2017. *Geochemistry and geochronology of the metabasites from the Posht-e-Badam region, Central Iran*, M.Sc. Thesis, Damghan University, School of Earth Sciences, 121 Pages (in Persian with English abstract).
- Lalonde, A.E. and Bernard, P., 1993. Composition and color of biotite from granites; two useful properties in characterization of plutonic suites from the Hepburn internal zone of Wopmay Orogen, Northwest Territories. *The Canadian Mineralogist*, 31(1), pp.203–217.
- Leake, B.E., Woolley, A.R., Birch, W.D., Burke, E.A., Ferraris, G., Grice, J.D., Hawthorne, F.C., Kisch, H.J., Krivovichev, V.G., Schumacher, J.C., Stephenson, N.C., 2003. Nomenclature of amphiboles: additions and revisions to the International Mineralogical Association's 1997 recommendations. *The Canadian Mineralogist* 41, 1355–1362.
 DOI: 10.2113/gscanmin.41.6.1355
- Leake, B. E., Woolley, A. R., Arps, C. E. S., Birch, W. D., Gilbert, M. C., Grice, J. D., Hawthorne, F. C., Kato, A., Kisch, H. J., Krivovochev, V. G., Linthout, K., Laird, J., Mandarino, J. A., Maresch, W. V., Nickel, E.H., Rock, N. M. S., Schumacher, J. C., Smith, D. C., Stephenson, N. C. N., Ungaretti, L., Whittaker, E. J. W., Youzhi, Gou (1997) Nomenclature of amphiboles: report of the Subcommittee on Amphiboles of the International Mineralogical Association, Commission on New Minerals and Mineral Names. *The Canadian Mineralogist*, 35 (1) 219–246
<https://doi.org/10.1180/minmag.1997.061.405.13>
- Ludwig, K.R., 2001. Eliminating mass-fractionation effects on U-Pb isochron ages without double spiking. *Geochimica et Cosmochimica Acta*, 65(18), pp.3139–3145.
[https://doi.org/10.1016/S0016-7037\(01\)00637-8](https://doi.org/10.1016/S0016-7037(01)00637-8)
- Ludwig, K.R., 2003. User's manual for Isoplot, v.3.00, a geochronological toolkit for Microsoft Excel. Berkeley Geochronological Center, Special Publication 4, 47–93.
- McCall, G.J.H., 1997. The geotectonic history of the Makran and adjacent areas of southern Iran. *Journal of Asian Earth Sciences* 15, 517–531.
- Majidi, J. and Baghbani, A. R., 2000. Geological map of the Ariz area (scale 1:100,000). Geological survey of Iran.
- McKibben, M.A., Shanks, W.C. and Ridley, W.I., eds., 1998. Applications of microanalytical

- techniques to understanding mineralizing processes (Vol. 7). Society of Economic Geologists.
- E. A. K. Middlemost 1985. *Magma and magmatic rocks. An introduction to igneous petrology*. 266 pp. London, New York: Longman. DOI: 10.1017/S0016756800026716
- Middlemost, E.A., 1994. Naming materials in the magma/igneous rock system. *Earth-science reviews*, 37(3-4), pp.215-224. [http://dx.doi.org/10.1016/0012-8252\(94\)90029-9](http://dx.doi.org/10.1016/0012-8252(94)90029-9)
- Moghadam, H. S., Li, X., Stern, R. J., Santos, J. F., Ghorbani, G. and Pourmohsen, M., 2016. Age and nature of 560–520 Ma calc-alkaline granitoids of Biarjmand, northeast Iran: insights into Cadomian arc magmatism in northern Gondwana, *International Geology Review*. <http://dx.doi.org/10.1080/00206814.2016.1166461>
- Moghadam, H.S., Li, X.H., Santos, J.F., Stern, R.J., Griffin, W.L., Ghorbani, G. and Sarebani, N., 2017. Neoproterozoic magmatic flare-up along the N. margin of Gondwana: The Taknar complex, NE Iran. *Earth and Planetary Science Letters*, 474, pp.83-96. <https://doi.org/10.1016/j.epsl.2017.06.028>
- Mollai, H., Dabiri, R., Torshizian, H. A., Pe-Piper, G., & Wang, W., 2019. Cadomian crust of Eastern Iran: evidence from the Tapeh Tagh granitic gneisses. *International Geology Review*, 64(10), 1372–1392. <https://doi.org/10.1080/00206814.2019.1670100>
- Monazzami Bagherzadeh. R., Karimpour, M. H., Lang Farmer, G., Stern. C. R., Santos, J. F., Rahimi, B. and Heidarian Shahri, M. R., 2015. U–Pb zircon geochronology, petrochemical and Sr–Nd isotopic characteristic of Late Neoproterozoic granitoid of the Bornaward Complex (Bardaskan-NE Iran), *Journal of Asian Earth Sciences* 111: 54 –71. <https://doi.org/10.1016/j.jseae.2015.05.019>
- Mutch, E.J.F., Blundy, J.D., Tattitch, B.C., Cooper, F.J. and Brooker, R.A., 2016. An experimental study of amphibole stability in low-pressure granitic magmas and a revised Al-in-hornblende geobarometer. *Contributions to Mineralogy and Petrology*, 171, pp.1-27. <https://doi.org/10.1007/s00410-016-1298-9>
- Nachit, H., Ibhi, A., Ohoud, M.B., 2005. Discrimination between primary magmatic biotites, reequilibrated biotites and neofomed biotites. *Comptes Rendus Geoscience* 337, 1415–1420. DOI: 10.1016/j.crte.2005.09.002
- Nachit, H., Razafigahefa, N.J.M.S., Stussi, J.M., Carron, J.P., 1985. Composition chimique des biotites et typologie magmatique des granitoides. *Comptes rendus de l'Académie des sciences. Série 2. Mécanique, Physique, Chimie, Sciences de l'univers, Sciences de la Terre* 301, 813–818.
- Nakamura, N., 1974. Determination of REE, Ba, Fe, Mg, Na, and K in carbonaceous and ordinary chondrites. *Geochemical et Cosmochimica Acta*, 38, 757-775. [https://doi.org/10.1016/0016-7037\(74\)90149-5](https://doi.org/10.1016/0016-7037(74)90149-5)
- Nouri, F., Davoudian, A. R., Allen, M. B., Azizi, H., Asahara, Y., Anma, R., ... & Khodami, M., 2021. Early Cambrian highly fractionated granite, Central Iran: Evidence for drifting of northern Gondwana and the evolution of the Proto-Tethys Ocean. *Precambrian Research*, 362, 106291. DOI: 10.1016/j.precamres.2021.106291
- Omrani, J., 1992. *Petrology and geochemistry of intrusions Zarrin area (Ardekan, Yazd)*. Unpublished M.Sc. Thesis, Tehran University, faculty of science (in Persian).
- Parvareh-Darbandi, M., Malekzadeh-Shafaroudi, A., Azim Zadeh, A.M., Karimpour, M.H., 2020. Magnetite mineralization properties of Narm iron mine with respect to petrology and geochemistry of its adjacent gabbroic-dioritic rocks (north of Tabas, South Khorasan Province). *Journal of Petrology*, 41:103-128. <https://doi.org/10.22108/jp.2020.118478.1145>
- Passchier, C.W. and Trouw, R.A., 2005. *Microtectonics*. Springer Science & Business Media.
- Pearce, J.A., 1983. Role of the sub-continental lithosphere in magma genesis at active continental margins, In: Hawkesworth CJ, Norry MJ, editors. *Continental Basalts and Mantle Xenoliths*. Nantwich, Cheshire: Shiva Publisher, pp. 230-249. <https://orca.cardiff.ac.uk/id/eprint/8626>
- Pearce, J.A., Harris, N.B. and Tindle, A.G., 1984. Trace element discrimination diagrams for the tectonic interpretation of granitic rocks. *Journal of Petrology*, 25(4), pp.956-983. DOI: 10.1093/petrology/25.4.956
- Pearce, J.A. and Peate, D.W., 1995. Tectonic implications of the composition of volcanic arc magmas. *Annual Review of Earth and Planetary Sciences*, Volume 23, pp. 251-286., 23, pp.251-286. 0048-6597/95/0515-0251\$05.00
- Peccerillo, A., & Taylor, S. R., 1976. Geochemistry of Eocene calc-alkaline volcanic rocks from the Kastamonu area, northern Turkey. *Contributions to mineralogy and petrology*, 58, 63-81.

- <https://doi.org/10.1007/BF00384745>
- Putirka, K., 2016. Amphibole thermometers and barometers for igneous systems and some implications for eruption mechanisms of felsic magmas at arc volcanoes. *American Mineralogist*, 101(4), pp.841-858. <https://doi.org/10.2138/am-2016-5506>
- Qiu, X., Liu, C., Mao, G., Deng, Y., Wang, F. and Wang, J., 2014. Late Triassic tuff intervals in the Ordos basin, Central China: Their depositional, petrographic, geochemical characteristics and regional implications. *Journal of Asian Earth Sciences*, 80, pp.148-160. <https://doi.org/10.1016/j.jseaes.2013.11.004>
- Ramezani, J. and Tucker, R.D., 2003. The Saghand region, central Iran: U-Pb geochronology, petrogenesis and implications for Gondwana tectonics. *American journal of science*, 303(7), pp.622-665. <http://dx.doi.org/10.2475/ajs.303.7.622>
- Rashidnejad Omran, N. A., Fattahi, A. A. and Masoudi, F., 2013. Petrography, Geochemistry, Origin and Tectonic Setting of Khoshoumi – DarAnjir Intrusive Complex, SW Saghand (Central Iran). *Scientific Quarterly Journal of Geosciences*, 22(86), 245-260. Doi: 10.22071/gsj.2012.54092\
- Rezaei, M. (2021). Petrology, geochemistry, isotope geology and geodynamic model of the Do-Chah metamorphic-igneous complex (SE Shahrood), Unpublished Ph.D. Thesis, Shahrood University of Technology, Faculty of Earth Sciences, 279 pages (in Farsi, with English abstract).
- Rezaei-Kakhkhaei, M., Corfu, F., Galindo, C., Rahbar, R. and Ghasemi, H., 2022. Adakite genesis and plate convergent process: Constraints from whole rock and mineral chemistry, Sr, Nd, Pb isotopic compositions and U-Pb ages of the Lakhshak magmatic suite, East Iran. *Lithos*, 426, p.106806. <https://doi.org/10.1016/j.lithos.2022.106806>
- Richards, J.P. and Kerrich, R., 2007. Special paper: adakite-like rocks: their diverse origins and questionable role in metallogenesis. *Economic geology*, 102(4), pp.537-576. <https://doi.org/10.2113/gsecongeo.102.4.537>
- Ridolfi, F., Renzulli, A., Puerini, M., 2010. Stability and chemical equilibrium of amphibole in calc-alkaline magmas: an overview, new thermobarometric formulations and application to subduction-related volcanoes. *Contributions to Mineralogy and Petrology* 160, 45–66.
- Ridolfi, F., 2021. Amp-TB2: An updated model for Calcic amphibole thermobarometry. *Minerals*, 11, 324. <https://doi.org/10.3390/min11030324>
- Rossetti, F., Nozaem, R., Lucci, F., Vignaroli, G., Gerdes, A., Nasrabadi, M., & Theye, T., 2015. Tectonic setting and geochronology of the Cadomian (Ediacaran-Cambrian) magmatism in central Iran, Kuh-e-Sarhangi region (NW Lut Block). *Journal of Asian Earth Sciences*, 102, 24-44. DOI: 10.1016/j.jseaes.2014.07.034
- Ruh, J.B., Le Pourhiet, L., Agard, P., Burov, E. and Gerya, T., 2015. Tectonic slicing of subducting oceanic crust along plate interfaces: Numerical modeling. *Geochemistry, Geophysics, Geosystems*, 16(10), pp.3505-3531. doi:10.1002/2015GC005998.
- Sabzehei, M., 2017. Geological map of Ali Abad (scale 1:25,000). Geological Survey of Iran, Tehran (In Persian).
- Sadeghian, M., Hosseini, S. H., Hemmati, A. and Shekari, S., 2017. Petrology, geochemistry and geochronology of SW Mayamey granitoids. *Scientific Quarterly Journal of Geosciences*, 26(103), 41-60. Doi: 10.22071/gsj.2017.46726
- Sarebani, N., 2017. Geochronology and Geochemistry of the granitoid rocks from the Taknar complex (NE Iran), M.Sc. Thesis, Damghan University, School of Earth Sciences, 168 Pages (in Persian with English abstract).
- Schandl, E. S., and Gorton, M. P., 2002. Applications of high field strength elements to discriminate tectonic setting in VMS environments. *Economic geology*. 97, 629-642. <https://doi.org/10.2113/gsecongeo.97.3.629>
- Shabanian, N., Davoudian, A. R., Dong, Y., & Liu, X., 2018. U-Pb zircon dating, geochemistry and Sr-Nd-Pb isotopic ratios from Azna-Dorud Cadomian metagranites, Sanandaj-Sirjan zone of western Iran. *Precambrian Research*, 306, 41-60. <https://doi.org/10.1016/j.precamres.2017.12.037>
- Shafaii Moghadam H., Xian-Hua Li X. H., Stern R. J., Ghorbani G., Bakhshizad F., 2016. Zircon U–Pb ages and Hf–O isotopic composition of migmatites from the Zanzan–Takab complex, NW Iran: Constraints on partial melting of metasediments, *Lithos*, Volumes 240–243, Pages 34-48, <https://doi.org/10.1016/j.lithos.2015.11.004>.

- Shand, S. J., 1943. Eruptive rocks; T. Murby and Co., London, 444p.
- Stein, E. and Dietl, E., 2001. Hornblende thermobarometry of granitoids of central Odenwald (Germany) and their implication for the geotectonic development of the Odenwald. *Mineralogy and Petrology*, 72, 185-207. <https://doi.org/10.1007/s007100170033>
- Stern, R.J., 2024. The Cadomian (~ 550 Ma) Orogen in North Africa and Arabia. *Journal of African Earth Sciences*, 215, p.105276. <https://doi.org/10.1016/j.jafrearsci.2024.105276>
- Sun, S. S., and McDonough, W. F., 1989. Chemical and isotopic systematics of oceanic basalts: implications for mantle composition and processes. Geological Society, London, Special Publications, 42(1), 313-345. <https://doi.org/10.1144/GSL.SP.1989.042.01.19>
- Tajbakhsh, G. (2020). 'Petrography, geochemistry and tectonic setting of mafic dyke swarms of Zarigan granitoid, north of Bafq (Central Iran)', *Scientific Quarterly Journal of Geosciences*, 30(117), pp. 175-188. Doi: 10.22071/gsj.2020.222632.1768
- Tajbakhsh G, Khodami M, Monsef R. 2023. Mineral chemistry and geothermobarometry based on amphibole of alkali gabbro dykes of Zarigan, northeast of Bafq. *www.ijcm.ir*; 31 (1) :59-74. URL: <http://ijcm.ir/article-1-1738-fa.html>
- Taki, S., Ganji A., Bafekr, N. 2013. Petrology and geochemistry of Lahijan granitoid according to new findings. *www.ijcm.ir* 2013; 21 (1):19-30. URL: <http://ijcm.ir/article-1-327-en.html>
- Trouw, R.A., Passchier, C.W. and Wiersma, D.J., 2009. Atlas of mylonites and related microstructures. Springer Science & Business Media. DOI: 10.1007/978-3-642-03608-8
- Tindle, A.G. and Pearce, J.A., 1981. Petrogenetic modelling of in situ fractional crystallization in the zoned Loch Doon pluton, Scotland. *Contributions to Mineralogy and Petrology*, 78, pp.196-207. <https://doi.org/10.1007/BF00373781>
- Uchida, E., Endo, S., Makino, M., 2007. Relationship between solidification depth of granitic rocks and formation of hydrothermal ore deposits. *Resource Geology* 57, 47–56. DOI: 10.1111/j.1751-3928.2006.00004.x
- Valeh N., and Haghipour, A., 1972. Geological map of Ardekan (scale 1:250,000), Geological Survey of Iran publication (in English).
- Vaziri, S. H., Majidifard, M. R. and Laflamme, M., 2019. New discovery on Ediacaran fossils from the Kushk Series in Bafq and Behabad regions, Central Iran. *Scientific Quarterly Journal of Geosciences*, 28(112), 261-268 (in Persian). Doi: 10.22071/gsj.2018.136508.1495
- Warr, L.N., 2021. IMA–CNMNC approved mineral symbols. *Mineralogical Magazine*, 85(3), pp.291-320. doi:10.1180/mgm.2021.43
- Wilson, M., 1989. Igneous Petrogenesis: A Global Tectonic Approach. Unwin Hyman, London, 466p. <https://doi.org/10.1007/978-1-4020-6788-4>
- Winter, J. D., 2010. An introduction to igneous and metamorphic petrology. Publisher: Prentice Hall, 2nd ed.
- Xianwu, B., Ruizhong, H., Hanley, J.J., Mungall, J.E., Jiantang, P., Linbo, S., Kaixing, W., Yan, S., Hongli, L., and Xiaoyan, H., 2009. Crystallisation conditions (T, P, fO_2) from mineral chemistry of Cu- and Au-mineralised alkaline intrusions in the Red River–Jinshajiang alkaline igneous belt, western Yunnan Province, China. *Mineralogy and Petrology*, 96, pp.43-58. DOI: 10.1007/s00710-009-0047-4
- Zolala, F., Alipour-Asll, M., Sadeghian, M., Ghasemi, H., Zhai, M. and Amidimehr, E., 2025a. Mineralogy, geochemistry, and petrogenesis of iron oxide-apatite ores in the Bafq mining district, Central Iran: Proposed a new tectonic setting for mineralization. *Journal of Geochemical Exploration*, 275, p.107785. <https://doi.org/10.1016/j.gexplo.2025.107785>
- Zolala, F., Sadeghian, M., Masood Alipour-Asll, M., Papadopoulou, L., Zhai, M., Foteini Aravani, F., Zhu, X. 2025 b. Petrography, mineral chemistry and geothermobarometry of monzogabbro-monzodiorite intrusions of N-NE Bafq: An approach to understanding of the Ediacaran-Cambrian intracontinental rift in the central part of Iran, accepted for publication or in press, *Geopersia Journal*, DOI. 10.22059/GEOPE.2025.393863.648816
- Zoleikhaei, Y., Cawood, P.A. and Mulder, J.A., 2025. Non-arc setting for “Cadomian” magmatism in Iran and Anatolia. *Geoscience Frontiers*, 16(2), p.101995. <https://doi.org/10.1016/j.gsf.2024.101995>
- Zoleikhaei, Y., Mazumder, R., Cawood, P. A., and De, S., 2023. Paleo-Mesoarchean magmatism and sedimentation in the northern part of the Singhbhum Craton: Evidence from zircon U-Pb-Hf, apatite U-Pb, and trace elements. *Precambrian Research*, 397, p. 107174.

<https://doi.org/10.1016/j.precamres.2023.107174>

Zoleikhaei, Y., Mulder, J.A. and Cawood, P.A., 2021. Integrated detrital rutile and zircon provenance reveals multiple sources for Cambrian sandstones in North Gondwana. *Earth-Science Reviews*, 213, p.103462. <https://doi.org/10.1016/j.earscirev.2020.103462>

Zoleikhaei, Y., Mulder, J.A. and Cawood, P.A., 2024. Early Paleozoic extensional tectonics along Gondwana's northern margin: Insights from Iran. *Gondwana Research*, 128, pp.106-126. <https://doi.org/10.1016/j.gr.2023.10.017>



This article is an open-access article distributed under the terms and conditions of the Creative Commons Attribution (CC-BY) license.